Searching for Better Photorefractive and Photovoltaic Materials

Objectives:

To discover better photorefractive organic materials with high performances and fast response time while simultaneously gaining a deeper understanding on their mechanisms. To synthesize novel conjugated diblock copolymers with build-in *p-n* junction for photovoltaic effect and molecular electronics.

Approaches:

We pursued three classes of organic photorefractive materials for a better understanding of the PR mechanism in organic materials, a faster response time, higher PR performance, lower applied field and a broader sensitive wavelength region: 1. monolithic molecular materials with tunable electronic properties, 2. conjugated oligomer-NLO chromophore system 3. PR polymers containing transition metal complexes as photosensitizers. Novel molecular structures will be synthesized and extensive physical studies will be performed. Issues related to these three classes of photorefractive materials will be addressed via new strategies. The synthesized materials will be sent to air force lab and other engineering groups for device exploration.

A series of asymmetric diblock conjugated copolymers (co-oligomers) will be synthesized and studied for photovoltaic effect and molecular electronics. These diblock copolymers contain both electron-rich and electron-deficient blocks and exhibit molecular *p-n* junction. New synthetic strategies of these materials will be developed. The phase separation behavior, optical and electronic properties of these block copolymers will be studied. Photovoltaic devices will be fabricated and their performance will be correlated with structural parameters. The energy difference between the built-in blocks will be varied with molecular structural modification to enhance the exciton dissociation efficiency. The absorption range of the conjugated copolymers can also be expanded to cover whole solar spectrum. Small oligomers of these molecules will be studied for molecular diode.

Papers published under partial support of AFOSR grant.

1. E. Chan and L. P. Yu "**Chemoselective immobilization of Gold Nanonanoparticles onto Self-Assembled Monolayers**" *Langmuire*, 18(2), 311-313, (2002).
2. H. B. Wang, M.-K. Ng, L. M. Wang and L. P. Yu "**Synthesis and Structural Characterization of Conjugated Diblock Copolymers**", *Chemistry - A European Journal*, 8, 3246-3253, (2002).
3. Chan, Eugene W. L.; Lee, Dong-Chan; Ng, Man-Kit; Wu, Guohui; Lee, Ka Yee C.; Yu, Luping. "**A Novel Layer-by-Layer Approach to Immobilization of Polymers and Nanoclusters.**" *J. Am. Chem. Soc.*, 124, 12238-12243, (2002).
4. Wei You, Liming Wang, Qing Wang and Luping Yu, " **Synthesis and Structure/Property Correlation of Fully Functionalized Photorefractive Polymers**", *Macromol.*, 35, 4636-4645, (2002).
5. Man-Kit Ng and Luping Yu, "**Synthesis of Amphiphilic Conjugated Diblock Oligomers As Molecular Diodes**", *Angew. Chem. Engl. Ed*, 41, 3598-3601, (2002).
6. Man-Kit Ng, Dong-Chan Lee & Luping Yu, "**Molecular Diodes Based Upon Conjugated Diblock Co-oligomers**", *J. Am. Chem. Soc.*, (2002), 124(40), 11862-11863.

7. You, Wei; Wang, Liming; Yu, Luping. **Novel synthesis of electron-deficient PPV and its application for photorefractive materials.** Polymer Preprints (American Chemical Society, Division of Polymer Chemistry) (2002), 43(2), 524-525.
8. Wang, Hengbin; Ng, Man-Kit; Yu, Luping. **Characterization of fully-conjugated diblock cooligomers.** Polymer Preprints (American Chemical Society, Division of Polymer Chemistry) (2002), 43(2), 518-519.
9. Yu, Luping; Wang, Hengbin. **Electroactive nanometer wires.** Polymer Preprints (American Chemical Society, Division of Polymer Chemistry) (2002), 43(2), 341-342.
10. Ng, Man-Kit; Wang, Liming; You, Wei; Yu, Luping. **Progress in fully functionalized organic photorefractive materials.** Proceedings of SPIE-The International Society for Optical Engineering (2002), 4462(Nonlinear Optical Transmission Processes and Organic Photorefractive Materials), 139-150.
11. Zhanjia Hou, Wei You and Luping Yu, "**Fine-Tuning Photorefractive Properties of Monolithic Molecular Materials**", *Appl. Phys. Lett.*, 82(20), 3385-3387, (2003).
12. You, Wei; Cao, Shaokui; Hou, Zhanjia; Yu, Luping. **Fully Functionalized Photorefractive Polymer with Infrared Sensitivity Based on Novel Chromophores.** *Macromolecules* (2003), 36(19), 7014-7019.
13. Yu, Luping. "**Conjugated diblock copolymers for molecular electronics and photonics.**" Polymeric Materials Science and Engineering, 88,169, (2003).
14. Yu, Luping; Ng, Man-Kit; Lee, Dong-Chang; Jiang, Ping; Morales, Gustavo. **Molecular diodes based on conjugated diblock oligomers.** Polymer Preprints (American Chemical Society, Division of Polymer Chemistry) (2003), 44(2), 375-376.
15. You, Wei; Hou, Zhanjia; Yu, Luping. **Fine-tuning photorefractive properties of moleculare photorefractive materials.** Polymer Preprints (American Chemical Society, Division of Polymer Chemistry) (2003), 44(2), 697-698.
16. Wei You, Zhanjia Hou and Luping Yu, " **Dramatic Enhancement of Photorefractive Properties by Controlling Electron Trap Density in a Monolithic Materials**", *Adv. Mater.*, (2004), 16, 356-360.
17. Hengbin Wang, Wei You, Ping Jiang and Luping Yu, H. Hau Wang, "**Supramolecular Self-Assembly of Conjugated Diblock Copolymers**", *Chem. Eur. J.*, (2004), 10, 986 -993
18. Dong-Chan Lee, Bong-Jun Chang, Young Ah Jang, Man-Kit Ng, Steven Heller and Luping Yu, "**Functional Polymers for Layer-by-Layer Construction of Multilayers via Chemoselective Immobilization**", *Macromol.*, (2004), 37(5), 1849-1856.
19. Ping Jiang, Gustavo M. Morales and Luping Yu, "**Synthesis of Diode Molecules and Their Sequential Assembly to Control Electron Transport**", *Angew. Chem. Int. Ed.*, (2004), *43*, 4471-4475.
20. Zhanjia Hou, Wei You and Luping Yu, "**Effect of a Trapping Molecule on the Monolithic Organic Photorefractive Materials**", *Appl. Phys. Lett.* (2004) *85*, 5221,
21. Xiangdong Qin, Tochko Tzvetkov, Xin Liu, Dong-Chan Lee, Luping Yu and Dennis C. Jacobs, **Site-Selective Abstraction in the Reaction of 5- to 20-eV O+ with a Self-assembled** Monolayer, *J. Am. Chem. Soc.*, 126, 13232-13233 (2004).
22. Wang, Hengbin; You, Wei; Yu, Luping. **Synthesis and structure/property correlation of cyano substituted oligo(phenylene vinylene)s.** Polymer Preprints (American Chemical Society, Division of Polymer Chemistry), (2004), 45(1), 187-188.
23. Dong-Chan Lee,1 Bong-Jun Chang,1 Luping Yu, Shelli L. Frey,1 Ka Yee C. Lee, Sirisha Patchipulusu, and Connie Hall, **Polymer Cushions Functionalized with Lipid Molecules**, *Langmuir.* (2004), 20, 11297.

24. Youngu Lee, Gustavo M. Morales and Luping Yu, "**Self-Assembled Monolayers of Isocyanides on Nickel Electrodes**, *Angew. Chem. Int. Ed.*, in press.
25. Wei You, Zhanjia Hou, and Luping Yu, Pronounced Photorefractiv Effect at Wavelength over 1000 nm in Monolithic Organic Materials, *Appl. Phys. Lett.*, in press.
26. Gustavo M. Morales, Ping Jiang, Shenwen Yuan, Youngu Lee, Arturo Sanchez and Luping Yu, "Inversion of the Rectifying Effect in Diblock Molecular Diodes by Protonation", *J. Am. Chem. Soc.*, 2005, in press.
27. Dong-Chan Lee, Gustavo M. Morales, Youngu Lee and Luping Yu, "Co-facial Porphyrin Multilayers via Layer-by-Layer Assembly", *J. Am. Chem. Soc.*, Submitted.

Summary of research achievements.

1. Detailed Studies of Photorefractive Effect in Monolithic Materials

In the area of electro-optical materials, photorefractive (PR) effect is a unique but complex phenomenon that involves four distinct processes: photocharge generation, charge transport, charge trapping, and build-up of space-charge field due to the redistribution of photogenerated charges and subsequent modulation of refractive index by space-charge field via the linear electro-optic (EO) effect, also known as the Pockels effect.[1-2] A photorefractive material therefore must possess both photoconductivity and EO effect. Although the PR effect was first discovered in inorganic ferroelectric single crystals in 1967, more investigation for organic PR materials have been carried on in the past decades due to their ease of fabrication and structural flexibility.[3-7] Numerous designing rationales have been implemented, resulting in a large database of materials, roughly categorized into composite materials[4] and fully-functionalized materials.[5-6]

Appeared recently, monolithic photorefrative materials have attracted more attention due to the simplicity of the materials and their appealing performance.[8-12] They are relatively easy to synthesize and purify, providing a good platform for the further understanding of the structure-property correlation and also the PR mechanism. They can be used either in bulk[8-9] or in doped form with typical photosensitizers such as C_{60} or TNFM.[10-12] Extensive studies have been focused on both steady state and dynamical photorefractive performance of these organic glasses.

More recently, our group found that certain nonlinear optical dye molecules could form homogeneous films and exhibit a large PR effect under an external electric field.[9] These are monolithic PR materials, containing only a single kind of molecules. These materials have numerous advantages over other types of organic photorefractive materials, such as high chromophore concentration, no phase separation, long-term stability, good optical quality, and ease of film fabrication. It is obvious that these molecules play all four functional roles required for the PR effect.

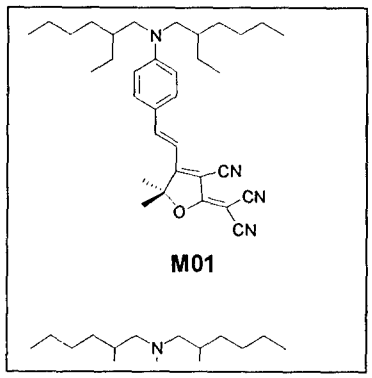

M01

Single component photorefractive materials based on small molecules have been synthesized. The side chains located in the electron-withdrawing group of these molecules were systematically changed in order to investigate their influence. It was demonstrated that the photorefractive performance of these materials could be fine-tuned by changing the length of the side chain. Excellent optical quality and photorefractive properties were obtained. A large net optical gain of $280cm^{-1}$ at a low external field (38.3 V/μm) and a diffraction efficiency of 82% were observed at 780 nm. The results indicate that an optimum side chain length exists for this type of molecules.

The molecular structures investigated are shown in Figure 1. The design idea of this molecule is similar to that of our previously reported system.[8] A tricyano-substituted furan group is used as the π electron acceptor, which renders this molecule highly hyperpolarizable. The R groups attached to the furan ring in this molecule can be modified to tune the physical properties of the resulting materials. The synthetic procedures of these molecules will be reported elsewhere. It was found that films with excellent optical quality could be prepared from these materials. As the R group

changes, the free volume and the interaction between chromophores are altered, which lead to changes in the glass transition temperature and PR properties.

Among the four materials shown in Table 1, **M01, M02** and **m06** are very stable. No crystallization and optical degradation was observed at room temperature for almost one year. But **m04** is stable only for one week at room temperature, after that, green crystals could be observed. Some physical and optical parameters of these materials were determined and summarized in Table 1. The glass transition temperature (T_g) was determined by a differential scanning calorimeter (Shimadzu, DSC 60). The Tg values of all the materials are close to or lower than room temperature and decreases as the side chain elongates. The films for our experiments were fabricated with heating the materials near the melting point and then sandwiching them by pressing two indium tin oxide (ITO) coated glass substrates. The thickness of the sample was pre-determined with the spacer used. The absorption coefficients of the samples were measured with a UV-visible spectrophotometer (Shimadzu UV-2401PC). The change of side chain does not affect conjugation length and has little influence on the absorption peak (Table 1). The resulting films are amorphous as confirmed with wide-angle X-ray diffraction experiments. These films are photoconductive, with dark current and photocurrent values listed in Table 1. The refractive index of the film was determined at 780nm with the prism-coupling method (Metricon model 2010 prism coupler).

Table. Molecules and their properties.

Compound	R	λ_{max} (nm) [$CHCl_3$]	α (cm^{-1})	n [780nm]	I_{dark}[a] (nA)	I_{photo}[a] (nA)	T_g (°C)	$E_{\pi/2}$ (V/μm)	$\Delta n(10^{-3})$ [$E_{\pi/2}$]	A_{BR}/A_{EO}
m0	Methyl	595.5	1.7	1.88	0.7	5.3	25.7	26	1.67	-2.9±0.4
m02	Ethyl	593.5	6.2	1.84	1.4	9.2	20.9	23	1.96	-5.0±0.8
m04	Butyl	592.5	1.2	1.83	2.7	9.9	17.6	23	1.85	-5.9±0.9
m06	Hexyl	593	1.4	1.8	35	42.7	8.8	23	1.69	-6.8±1

a. Note: Photoconductive measurements were performed with samples of 27 μm-thickness at an external field of 30V/μm; the irradiation intensity of the light was 103 mW/cm^2 at 780 nm.

Photorefractive gain and diffraction efficiency were determined with two-beam coupling and degenerated four-wave mixing experiments. The PR properties of **m06** were investigated at 20°C due to probable dielectric breakdown at a high electric field at room temperature, and the others were investigated at 25°C. As a standard method for two-beam coupling, the two P-polarized laser beams, with intensities of $I_1(0)$ and $I_2(0)$, were overlapped in the film to write the grating. The sample was tilted at 53°, with an external intersect angle of 18°. The intensities, $I_1(L)$ and $I_2(L)$, behind the sample were measured as a function of applied field. With an increasing applied field, $I_1(L)$ increases and $I_2(L)$ decreases superlinearly. The incident two-beam intensities were equal, $302mW/cm^2$. The gain coefficient was calculated by using the expression,

$$\Gamma = [\ln(\gamma\beta) - \ln(\beta + 1 - \gamma)]/L \qquad (1)$$

where L is the optical path length for beam I_1, β is the ratio of the two input beam intensities, $\beta = I_2(0)/I_1(0)$, γ is the beam coupling ratio defined as the ratio of intensities of $I_1(L)$ with and without the presence of I_2, $\gamma = I_1(L)_{(I2\neq 0)}/I_1(L)_{(I2=0)}$.

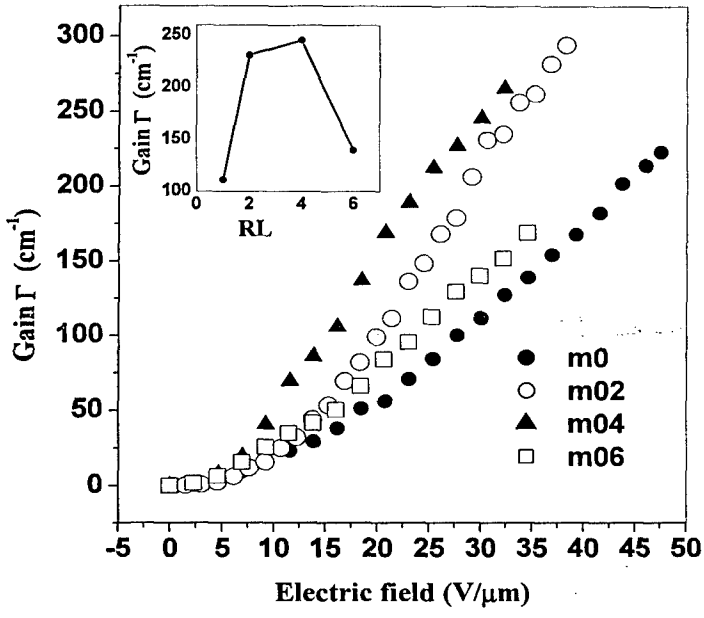

FIG. 2. Optical gain as a function of applied field. The inset is the change of optical gain at 30v/μm versus the relative length of side chain (RL). The solid line is a guide to eye

The dependence of the gain coefficients on the external field for the samples is shown in Figure 2. The data were collected before the dielectric breakdown of the samples at a high external field. The net optical gains were obtained at an electric field as low as 5V/μm for all four materials. At high electric field, large net optical gains were observed for all samples. For example, a gain value for molecule **m02** reached 285 cm^{-1} at a field of 38.3V/μm, which is almost as large as six times the value of the monolithic PR materials we reported before at the same electric field, and comparable with the best composite materials and low molecular weight PR materials doped with sensitizer.[10-11] The inset in Figure 2 shows the change of optical gain for different materials with relative lengths of side chains at an electric field of 30V/μm. It shows that side chains with ethyl and butyl groups could significantly improve photorefractive properties. These experimental results could be easily understood if we consider the difference between molecular structures and T_g values. As the size of side chain increases, the intermolecular interactions could be weakened and T_g values decrease correspondingly, which will benefit the chromophore's orientation and reorientation under the combined external electric field and space charge field. The optical gain measurements with S-polarized light and response time (showed in figure 4 below) support this point. The calculated contribution of birefringence and electro-optical effect to the index modulation, A_{BR}/A_{EO} (in Table 1), increases as the Tg decreases.[12] However, as the size of the side chain increases, the concentration (N) of the effective nonlinear optical chromophores decreases and the molecular weight (M) increases, which leads to the decreases of the figure of merit of molecule F, $F=(9K_BT\mu\beta+2\mu^2\Delta\alpha)/K_BTM)$.[13] It is well known that the refractive index modulation, Δn, is

proportional to the N and F.[3, 5] Therefore, considering the two integrated effects, an optimized side chain length exists for this type of material.

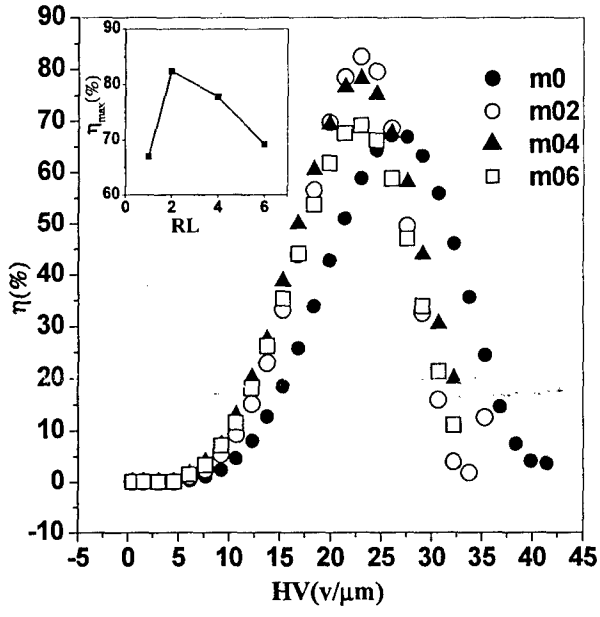

FIG. 3. Diffraction efficiencies as a function of applied field. The inset is maximum diffraction efficiencies versus the relative length of side chain (RL). The solid line is a guide to eye

Degenerated four wave mixing experiments were performed with two s-polarized beams at an equal intensity of 302 mW/cm^2, overlapped in the film to write the grating. A weak p-polarized reading beam with an intensity of 16.9 mW/cm^2 was counter-propagated to one of the writing beams to detect the process of grating build-up. The normal of the surface was tilted 53° with respect to the symmetric axis of the two intersected beams and the external internal beam angle was 18°. The diffraction efficiency is defined as the ratio between the intensity of the diffracted beam and the transmitted beam intensity in the absence of the two writing beams. The field dependence of the diffraction efficiencies for the different materials is shown in Figure 3. Large diffraction efficiencies and low $E_{\pi/2}$ values (the applied fields at the maximum diffractions) were observed. The inset in Figure 3 shows the change of maximum diffraction efficiency (η_{max}) for different materials versus the relative length of the side chain. The refractive–index modulations (Δn) also were determined at $E_{\pi/2}$ (in table 1) according to the expression [9]

$$\Delta n = \lambda \sqrt{\cos\theta_1 \cos\theta_2}\, \sin^{-1} \sqrt{\eta} / \pi d \cos(\theta_2 - \theta_1) \qquad (2)$$

where d is sample thickness, λ is the wavelength, and θ_2 and θ_1 are the incident internal angles of the two writing beams. The same trend as the photorefractive gain can be observed, except in material **m04,** in which crystallization may have caused lower diffraction efficiency due to scattering.

The response times of grating buildup were measured as follows. The field was applied and one writing beam and reading beam illuminated the samples. After about 10-15 minutes, the other writing beam was applied and the diffracted reading beam was monitored. We found that the dynamics of

grating formation do not follow a single-exponential function since two processes contribute to the diffraction signal, the internal electric field build-up, and reorientation of the nonlinear molecules under the internal electric field. Therefore the diffraction signal was fitted with the bi-exponential function,[14]

$$\eta(t) = \eta_0[1 - \{a\exp(-t/\tau 1) + (1-a)\exp(-t/\tau 2)\}]^2 \qquad (3)$$

where η_0 is the steady-state diffraction efficiency, $\tau 1$ corresponds to the time of internal electric field buildup, τ_2 is the reorientation time of the nonlinear molecules with the internal electric field and a is a dimensionless weighting factor. Figure 4 shows the response times, $\tau 1$ and $\tau 2$, as a function of the relative length of side chain. As the side chain lengthens, the reorientation time of the chromophores, τ_2, decreases significantly. The decrease in τ_2 is mainly due to the lower glass transition temperature in materials and the weakened interaction between molecules with longer side chains. The variation in τ_1 values was small, which is expected because the side chain substitution did not change the electronic properties of the molecules.

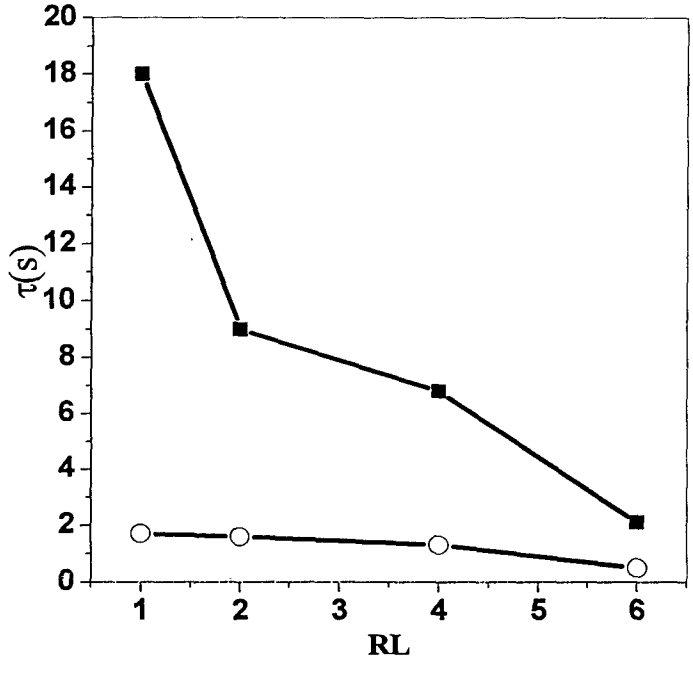

FIG. 4. The change of response time $\tau 1$ (bottom circle) and $\tau 2$ (top, filled circle) different samples versus the relative length of side chain. The solid line is a gu to eye

References:

[1] W. E. Moerner and S. M. Silence, Chem. Rev. **94**, 127 (1994).
[2] S. Ducharme, J. C. Scott, R. J. Twieg, and W. E. Moerner, Phys. Rev. Lett. **66**, 1846 (1991).
[3] W. E. Moerner, A. Grunnet-Jepsen, and C. L. Thompson, Annu. Rev.Mater. Sci. **27**, 585 (1997).

[4] P. Cheben, F. del Monte, D. J. Worsfold, D. J. Carlsson, C. P. Grover, J. D. Mackenzie, Nature **408**, 64 (2000)
[5] S. J. Zilker, ChemPhysChem, **1**, 73 (2000).
[6] L. P. Yu, W. K. Chen, Z. H. Peng, and A. R. Gharavi, Acc. Chem. Res. **29**, 13 (1996)
[7] Q. Wang, L. Wang, L. Yu, J. Am. Chem. Soc. **120**,12860 (1998).
[8] W. You, L. Wang, Q. Wang, L. Yu, Macromolecules, **35**, 4636 (2002)
[9] L. Wang, M.K. Ng, and L. Yu, Appl. Phys. Lett. **78**, 700 (2001).
[10] D. Wright, U. Gubler, Y. Roh, W. E. Moerner, M. He, R. J. Twieg, Appl. Phys. Lett., 79, 4274(2001).
[11] U. Gubler, M. He, D. Wright, Y. Roh, R. Twieg, W.E. Moerner, Adv. Mater. 14, 313(2002)
[12] W. E. Moerner, S. M. Silence, F. Hache, and G. C. Bjorklund, J. Opt. Soc. Am. B **11**, 320 (1994).
[13] Figure of merit of molecule $F=(9K_BT\mu\beta+2\mu^2\Delta\alpha)/K_BTM$, in which, K_B is the Boltzmann's constant, T is the absolute temperature, μ is the dipole moment, $\Delta\alpha$ is the difference of first-order polarizability parallel and perpendicular to the molecular axis, β represents the second-order polarizability along axis of the dipole moment and M molecular weigh. Since the side chains do not influence the charge distribution and conjugation length as we stated in the text, we assume here that parameters,μ,β, $\Delta\alpha$, are the same for the four molecule we studied.
[14] G. Bauml, S. Schoter, U. Hofmann, and D. Haarer, Opt. Commun. **154,** 75 (1998)

2. Influence of Experimental Conditions on PR Effect:

Since PR effect is a complicated physical phenomenon, many experimental parameters will affect the PR performances of the materials, such as working wavelength, light intensity and index grating spacing. The dependence of PR performances, including optical gain Γ, diffraction efficiency η and response time τ, on experimental conditions also reveal many intrinsic properties of the materials. From the above studies, we found the molecule **M02** with ethyl groups is the best in terms of its high gain and diffraction efficiency at low fields, as well as the good thermal stability. Therefore, molecule **2** was chosen for the comprehensive study of the influence of experimental conditions on its PR properties.

The important parameter of a PR material, optical gain, was deduced by using expression

$$\Gamma = [\ln(\gamma\beta) - \ln(\beta + 1 - \gamma)]/L \qquad (1)$$

where L is the optical path length for beam I_1, β is the ratio of the two input beam intensities, $\beta = I_2(0)/I_1(0)$, γ is the beam coupling ratio defined as the ratio of intensities of $I_1(L)$ with and without the presence of I_2, $\gamma = I_1(L)_{(I2\neq 0)}/I_1(L)_{(I2=0)}$. Another characteristic, the diffraction efficiency, is deduced according to equation

$$\eta = 100 \cdot I_s/I_p \qquad (2)$$

I_s is the intensity of the diffracted beam and I_p is the transmitted beam intensity in the absence of the two writing beams. Assuming the internal electric field increases exponentially, we can obtain response time by fitting the dynamic diffraction signal based on the equation [1]

$$\eta(t) = \eta_0[1 - \{a\exp(-t/\tau 1) + (1-a)\exp(-t/\tau 2)\}]^2 \qquad (3)$$

where η_0 is the steady-state diffraction efficiency, τ_1 corresponds to the time of internal electric field buildup, τ_2 is the reorientation time of the nonlinear molecules with the internal electric field and a is a dimensionless weighting factor.

According to the Kukhtarev's model, [2,3]

$$\Gamma \propto E_{sc} \cdot \sin\Phi \qquad (4)$$

E_{sc} is the internal electric field due to the light pattern modulation and Φ is the phase shift between the internal electric field E and light intensity pattern

$$E_{sc} = m \cdot E_q \cdot \left(\frac{E^2 + E_D^2}{E^2 + (E_D + E_q)}\right)^{1/2} \cdot \frac{\sigma_{ph}}{\sigma_{Dark} + \sigma_{ph}} \qquad (5)$$

$$\Phi = \arctan\left(\frac{E^2 + E_D^2 + E_D \cdot E_q}{E \cdot E_q}\right) \qquad (6)$$

where m is the light modulation, $E_q = eN_{eff}/\varepsilon_0 \varepsilon K_G$ is the trap-limited space-charge field, $E_D = K_B T K_G/e$ is the diffusion field, $E = E_0 \sin\theta_{tilt}$, σ_{ph} and σ_{Dark} are photoconductivity and dark conductivity, e is the charge of an electron, K_B is the Boltzmann's constant, T is the absolute temperature, $K_G = 2\pi/\Lambda$ is the grating wave vector, ε_0 is the permittivity of free space, ε is the relative permittivity, E_0 is the external electric field, N_{eff} is the effective trap density, Λ is the grating spacing, θ_{tilt} is the grating tilt angle with respect to the normal of the sample.

For p-polarized probe beam based on our oblique experimental condition, based on the Kogelnik's theory, diffraction efficiency can be approximated as shown below [4]

$$\eta \propto \sin^2\left(\frac{\pi \cdot E_{sc} \cdot L \cdot \cos(\theta_2 - \theta_1)}{\lambda \cdot n \cdot (\cos\theta_2 \cdot \cos\theta_2)}\right) \qquad (7)$$

a. Grating spacing (Λ) dependence of PR properties. The dependence of optical gain on grating spacing was studied in both inorganic and organic materials to abstract important information on trap density. The optimum grating spacing Λ was reported about 1 μm for many organic materials,[5,6] and the length scales of charge transport in organic PR materials were deduced with different experimental methods.[7-9] It should be noted that different materials have the different carrier drift lengths, which may lead to different optimum Λ for optimized PR properties. According to the PR theory, equation (4)-(6), the PR gain Γ is closely related to N_{eff}. It is predictable that the internal electric field (E_{sc}) will increase and phase shift will decrease with the increase in Λ (the θ_{tilt} was kept constant to exclude the influence of E). Therefore both E_{sc} and Φ will determine the grating spacing value Λ_{peak} at which the maximum gain coefficient is observed. Fig.5a shows the theoretical curve of the gain Γ as a function of Λ under an assumed N_{eff} (the parameters used are ε=8, θ_{tilt}=25°, E_0=23V/μm). We found Λ_{peak} is sensitive to N_{eff} at a fixed θ_{tilt}. The effective trap density, N_{eff}, can be deduced by fitting the curve of gain Γ versus Λ. Fig. 5Ab shows experimental results of the gain versus Λ for different θ_{tilt} (two p-polarized beam intensities I_1=I_2=310mw/cm^2, E_0=23V/μm). We indeed found different Λ_{peak} at different tilt angle. For example, Λ_{peak} is about 3.2 μm at θ_{tilt}=15°, but about 5.3 μm at θ_{tilt}=25°. The results of theoretical fitting (solid lines in Fig. 5Aa, according to equation (4)) showed almost the same N_{eff}, 5.5±0.5×10^{15}cm^{-3}, for different θ_{tilt}. This value is smaller than the values of other PR materials reported.[5,10-11] It is reasonable since our monolithic material is very pure and exhibits low intrinsic traps (the impurities in organic materials are considered one of the major reasons to act as traps). Using the data we obtained before[12] A_{BR}/A_{EO}≅-5±0.5, and by fitting the curves, we determined the contribution constants of electric-optic (EO) effect C_{EO}=0.39±0.1×10^{-17} m^2/V^2 and birefringence (BR) effect C_{BR}=1.26±0.3×10^{-17}m^2/V^2, which are almost two orders of magnitude larger than those values reported for PR polymers.[5] The large values is consistent with the high density of chromophores in our monolithic materials (about 6×10^{21}molecules/cm^3) since the two factors (C_{EO} and C_{BR}) are proportional to the chromophore density.[3] They also predict the relative low $E_{\pi/2}$ at which the over-modulation occurs as confirmed in experiment since $E_{\pi/2}$ is inversely proportional to the C_{EO} and C_{BR}. Fig.5Ac shows the diffraction efficiency as a function of the grating spacing (two p-polarized beam intensities I_1=I_2=310mw/cm^2, s-polarized beam I_3=5mW/cm^2, θ_{tilt}=25°, E_0=23V/μm). Unlike the gain coefficient, the diffraction efficiency tends to saturate, which is also in accordance to the theoretical prediction of equation (7) (solid line in Fig.1c. with the N_{eff} we obtained above). Because longer grating spacing requires larger electric field to move charge carrier, the experimental results showed that the $E_{\pi/2}$ increases with the lengthening the grating spacing (inset of Fig. 5Ac). Fig.1d shows the response time versus Λ (the same experimental conditions as Figure 5Ac). The results are in contrary to what we expected that the shorter the grating spacing, the faster the response time. In fact, there seems to be an optimum grating spacing to achieve the fastest response time, for both τ_1 and τ_2. The grating spacing at which the fastest response time was observed is almost the same as the Λ_{peak} indicated in Fig. 5Ab. This grating spacing value maybe corresponds to the drift length of charge carrier. This conclusion needs to be further confirmed with the independent experiments.[7]

b. Tilt angle dependence of the PR properties. For the organic PR material, it is well known that the quantum efficiency of charge generation is highly field dependent. The external electric field plays two roles: to induce the chromophore orientation and to separate the electron-

hole pair (a Frankel exciton) to generate free charges for creating space charge field. To assist charge separation, only the electric field component on the grating vector plays the effective role. Therefore for the measurement, the sample needs to be tilted with an angle (θ_{tilt}) with respect to the symmetric axis of the two intersected beams. From the equation (4) and (7), we can see that the gain Γ and diffraction efficiency η are closely related to θ_{tilt}. Fig. 5Ba is the theoretical curves of E_{sc} and Φ versus θ_{tilt} (parameters used are N_{eff}=5.5±0.5×10^{15}cm^{-3}, Λ=3.6 μm, E_0=23V/μm). It shows that, for certain N_{eff}, the E_{sc} and Φ increase exponentially and tend to saturate with further increase in θ_{tilt}. Fig. 2b shows the experimental results of Γ versus θ_{tilt} (two p-polarized beam intensities I_1=I_2=310mw/cm^2, E_0=23V/μm, Λ=3.6 μm). The solid line in Fig. 5Bb is the theoretical fitting with equation (4) using the data C_{EO} and C_{BR} obtained above, from which N_{eff}=3.5±0.5×10^{15}cm^{-3} was determined. For the diffraction efficiency, both experimental and theoretical results show increases with tilted angle and then saturates (Fig. 5Bc). An effective trap density, N_{eff}, of 4±0.5×10^{15}cm^{-3} was obtained after fitting. It is interesting to note that the $E_{\pi/2}$ decreases with the increase in θ_{tilt}. This could be easily explained since E and γ_{eff} are both proportional to sin(θ_{tilt}).[5] The response time, τ_1 and τ_2, almost decrease linearly with the increase in θ_{tilt}. Although the large tilt angle will benefit the PR properties, the loss due to the reflection will also increase, which will add additional uncertainty to the experimental results. This uncertainty may also cause the slight difference of N_{eff} obtained from different experiments. On the other hand, the maximum internal incident beam angle will also restrict the PR property improvement.[8] Considering all the factors, the tilt angle of 25° was chosen for our further experiments.

c. Intensity dependence of PR properties. According to equation (6), if the dark conductivity is very small, the gain and diffraction efficiency have no relationship with the intensity (σ=neμ=e$\mu\phi\alpha\tau$I/hν). However, a linear or sublinear relationship was observed between the response speed and intensity in these monolithic materials.[13,14] Fig.5Ca shows the experimental results of gain versus the total incident intensity (the experimental condition are two p-polarized beam intensities I_1=I_2, Λ=3.7 μm, θ_{tilt}=25°, E_0=23V/μm). In order to explain the dependence of gain as a function of incident intensity, we now consider the simplified charge generation equation in PR theory.[2] Assuming there are no other factors (such as deep traps) affecting the charge density and the electron density n_e is equal to the hole density n_h, n_e=n_h=n, the temporal evolution of n is given by the following equation

$$dn/dt = sI(N-n) - \gamma n^2 \qquad (8)$$

where N is the total number density of carriers available to be excited (here N=N_{eff}), s is the cross section for photoexcitation and γ is the recombination coefficient. The solution of this equation predicts a dependence of the gain, diffraction efficiency and response time on the light intensity since all of these parameters are related to the excited charge density. At certain poling field, the gain Γ is proportional to the excited carrier density. We then can derive the relation

$$\Gamma \propto \frac{1}{1/2N + [\gamma/sNI + 1/4N^2]^{1/2}} \qquad (9)$$

Based on the N_{eff} value obtained above, N=N_{eff}=5.5±0.5×10^{15}cm^{-3}, by fitting experimental results with equation (9) (solid line in Fig.5Ca), the fitted value is γ/s=4×10^{-15}cm·mW. This value predicts that the gain increases as a sub-linear function of intensity at very low intensity and tends to saturate at high intensity. For the material we studied, the threshold is about 200mW/cm^2. This conclusion is also supported by the experimental results on diffraction efficiency. The diffraction efficiency was measured with the same experimental conditions described above, except that the two writing beams are s-polarized and the probe beam is p-polarized with intensity of 5mW/cm^2. Fig. 5Cb

shows the experimental results where the threshold about 200mwW/cm^2 also exists. The diffraction efficiency versus intensity exhibit the relation as

$$\eta \propto \left(\frac{1}{1/2N + [\gamma/sNI + 1/4N^2]^{1/2}} \right)^2 \qquad (10)$$

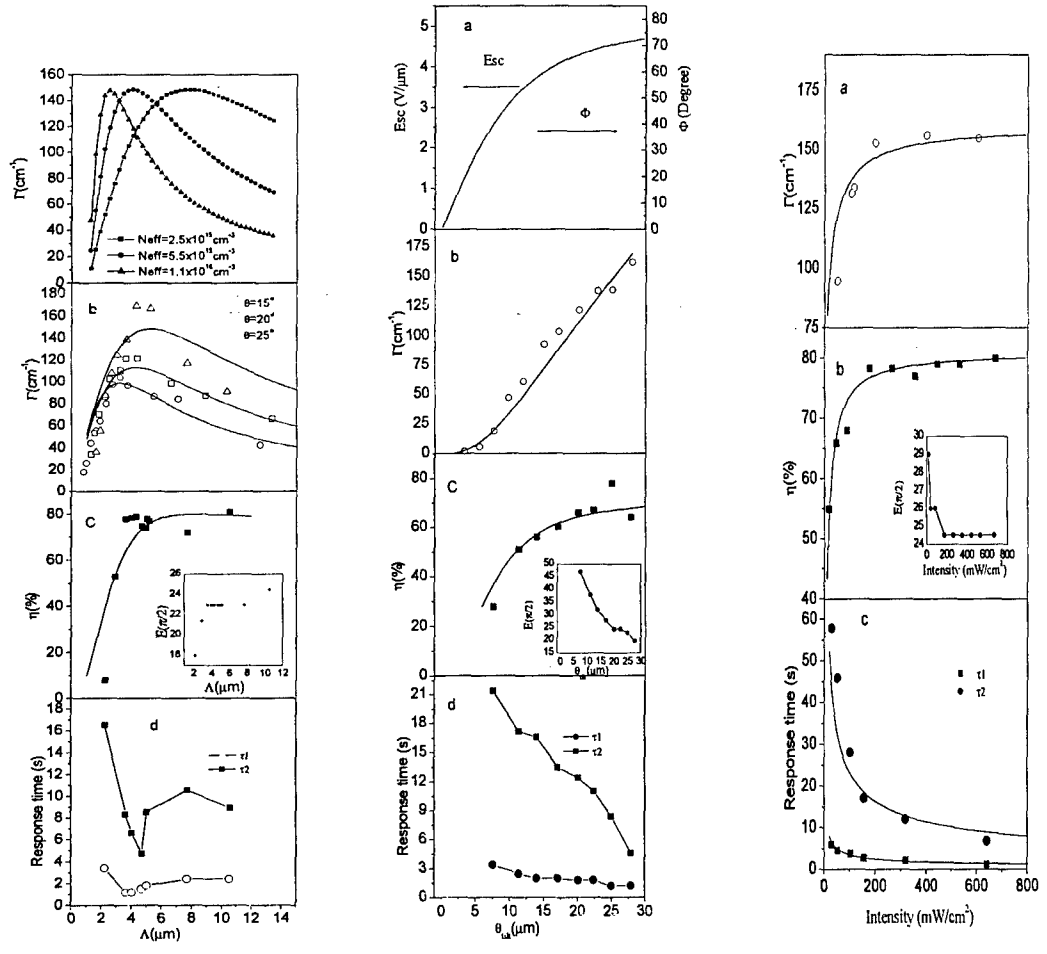

A. B. C.

Figure 5. Photorefracive effect as functions of experimental conditions. A. effect of grating spacing, B. effect of sample tilted angle, C. effect of light intensity.

γ/s=1×10^{-15} cm·mW was obtained, which is smaller than the value obtained above. The difference may be due to the experimental uncertainty (such as sample thickness, sample history). At the same time, $E_{\pi/2}$ also decreases with increasing the incident intensity. It is plausible that the stronger the incident intensity, the more the excited photo-charges, and the lower poling electric field needed to move the charge carrier due to aforementioned reasons. It was predicted that light intensity would affect response. Fig. 5Cc is the response time versus the incident intensity (the same experimental conditions as Fig. 5Cb). Both the fast and the slow response time constants decrease with the increase in the intensity, but at certain intensity value, both of them are almost saturated and a threshold also exists. The behavior of response time can be explained with model introduced above.

Based on the parameters we obtained (N=5±0.5×10^{15}cm^{-3}, γs=1×10^{-15} cm·mW), the solid lines in Fig. 5Cc is the theoretical fitting with the following relation

$$\tau \propto \frac{1}{[\gamma sNI + (sI/2)^2]^{1/2}} \qquad (11)$$

The fitting parameters are s=0.01cm^2/mJ, γ=1×10^{-17}cm^{3}s^{-1}. Compared with inorganic materials, such as BSO crystal, the cross section for photoexcitation is lager (s_{BSO}=1.06×10^{-5}m^{2}J^{-1}), while the recombination coefficient $\gamma$is smaller (γ_{BSO}=1.65×10^{-17}m^{3}s^{-1}). This means the photocharge carrier is easier to produce for our material, which is in accordance to the low $E_{\pi/2}$ we observed.

Reference:

1. Solymar, L.; Webb, D. J.; Grunnet-Jepsen, A. *The Physics and Applications of Photorefractive Materials* Clarendon Press, Oxford, **1996**.
2. Günter, P.; Huignard, J. P.; Eds. *Photorefractive Materials and Their Applications* Springer-Verlag, Berlin, **1988**, Vols. 1 and 2.
3. Moerner, W. E.; Silence, S. M. *Chem. Rev.* **1994**, *94*, 127.
4. Moerner, W. E.; Grunnet-Jepsen, A.; Thompson, C. L. *Annu. Rev. Mater. Sci.* **1997**, *27*, 585.
5. Yu, L.; Chan, W. K.; Peng, Z. H.; Gharavi, A. *Acc. Chem. Res.* **1996**, *29*, 13.
6. Yu, L. *J. Polym. Sci. Part A: Polym. Chem.* **2001**, *39*, 2557.
7. Zhang, Y.; Burzynski, R.; Ghosal, S.; Casstevens, M. K. *Adv. Mater.* **1996**, *8*, 111.
8. Wang, L.; Ng, M.-K.; Yu, L. *Appl. Phys. Lett.* **2001**, *78*, 700.
9. Hou, Z.; You, W.; Yu, L. *Appl. Phys. Lett.* **2003**, *82*, 3385.
10. Gubler, U.; He, M.; Wright, D.; Roh, Y.; Twieg, R.; Moerner, W. E. *Adv. Mater.* **2002**, *14*, 313.
11. Ostroverkhova, O.; Wright, D.; Gubler, U.; Moerner, W. E.; He, M.; Sastre-Santos, A.; Twieg, R. J. *Adv. Funct. Mater.* **2002**, *12*, 621.
12. Ostroverkhova, O.; Moerner, W. E.; He, M.; Twieg, R. J. *Appl. Phys. Lett.* **2003**, *82*, 3602.
13. Melikian, G.; Rouessac, F.P.; Alexandre, C. *Synth. Commun.* **1995**, *25*, 3045.
14. Zhang, C.; Wang, C.; Dalton, L. R.; Zhang, H.; Steier, W. H. *Macromolecules* **2001**, *34*, 253.
15. He, M.; Leslie, T. M.; Sinicropi, J. A. *Chem. Mater.* **2002**, *14*, 2393.
16. Wright, D.; Gubler, U.; Roh, Y.; Moerner, W. E.; He, M.; Twieg, R. J. *Appl. Phys. Lett.* **2001**, *79*, 4274.
17. Moerner, W. E.; Silence, S. M.; Hache, F.; Bjorklund, G. C. *J. Opt. Soc. Am. B* **1994**, *11*, 320.

3. Dramatic Enhancement of Photorefractive Properties by Controlling Electron Trap Density in a Monolithic Material

To optimize the photorefractive performance, each process in the photorefractive effect, including charge generation, migration, trapping and space-charge field modulation of refractive index via linear electro-optical effect, has to be fine-tuned.[4] Intensive studies of structure-property relation of nonlinear optical chromophores, different conductive polymer backbones and photosensitizers have thus been conducted in the past years. Few studies were reported for intentional control of trapping density[5] which is crucial in the build-up of the space charge field. This is due to the difficulty in evaluating the impurities, structural defects etc. in a polymer sample, which serve as the charge trapping sites in organic PR materials.[6]

We discovered the monolithic PR small molecules whose major charge carriers are electrons.[7] More recently, we found small molecule **M01** exhibiting a net optical gain up to 182 cm^{-1} at a field of 41.5V/μm.[8] Because these are monolithic small molecular systems, materials can be purified very carefully. This provides us with an opportunity to investigate the effect of concentration of trapping centers by deliberately adding certain well-designed dopants. In this communication, we report the control of electron trapping density and improved PR properties for the first time.

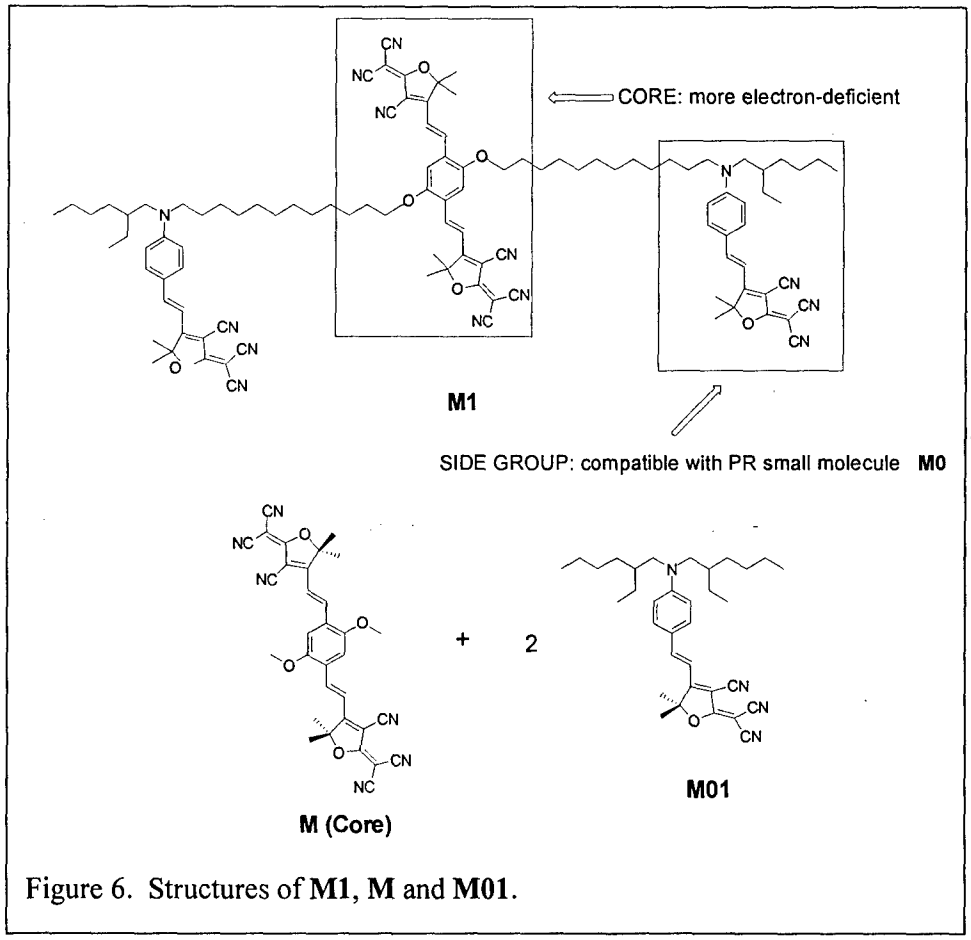

Figure 6. Structures of **M1**, **M** and **M01**.

In this work, we use materials made from **M01** as the basic material. The success of electron trapping relies on the synthesis of the molecule **M1** whose core part (**M** in Figure 6) contains six cyano groups, and is more electron-deficient than the side groups which are basically **M01**. When

electrons are generated by illumination, they will be trapped by the core part of **M1**. And the introduction of side groups mimicking **M01** could be used to prevent the possible phase separation for the mixture of **M01** and **M1**, ensuring the miscibility of **M1** and **M01** due to structure similarity.

UV-Vis spectra of all three molecules correctly reflect the structural relationship. Compared with the absorption maximum (594nm) of **M01**, the major absorption band of **M** appears around 534nm. For **M1** combining **M** and **M01**, absorption peaks corresponding to structurally similar parts can be observed.

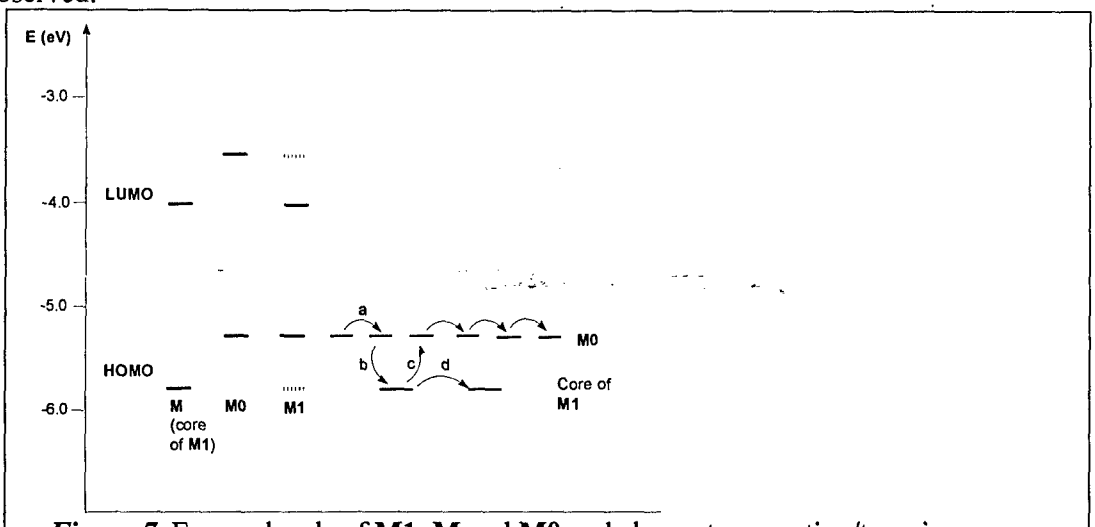

Figure 7. Energy levels of **M1**, **M** and **M0** and charge transporting/trapping mechanism: (a) transport

The key proof for the electron trapping by **M1** can be obtained by using the cyclic voltammetry from which the redox potentials for different molecules can be deduced. The HOMO energy of molecule **M** was determined to be –5.827eV, which is lower than HOMO energy of **M01** (–5.289eV) by 0.538eV; the LUMO energy of **M** (–4.048eV) is lower than the LUMO energy of **M01** (–3.588eV) by 0.46eV. The redox potentials of **M1** correctly reflect the structural similarity with **M** and **M01** with all the possible energy levels. The electrochemical gap coincides with the optical gap derived from the UV-Vis spectrum. Based on these results, a schematic view of the energy levels is shown in Figure 7.

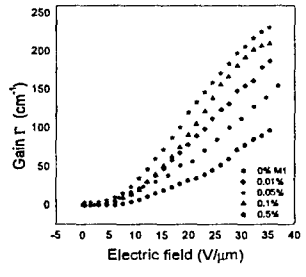

Figure 8. Dependence of the gain coefficients Γ from 2BC on applied field.

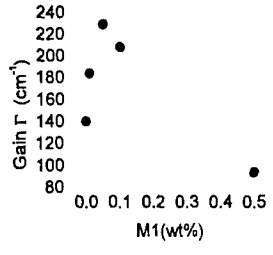

Figure 9.Dependence of the gain coefficients Γ with **M1** concentration at applied field of 35V/μm.)

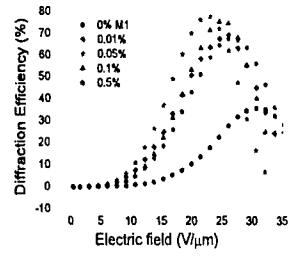

Figure 10. Applied field dependence of the diffraction efficiency from DFWM. experiment.

Photorefractive measurements were conducted on a film sandwiched between two indium-tin oxide (ITO) glass electrodes with thickness controlled by a polyimide spacer of 125μm. Samples with different weight percentage of **M1** over **M0** were obtained by dissolving appropriate amounts of **M1** and **M0** into methylene chloride into homogeneous solution followed by complete removal of solvent by vacuum for 24 hours. Five samples were prepared where **M1** concentration equals to 0, 0.01%, 0.05%, 0.1%, and 0.5%. Two beam coupling (2BC) experiments were performed to obtain the gain coefficients (Γ) for all the materials (Figure8). Figure 9 shows the dependence of optical gain on the concentration of trapping molecule. Since the absorption coefficients (α) for all the materials are 1.9, 2.7, 2.5, 5.9, and 10.8cm^{-1} for the samples of increasing **M1** concentration, respectively, all of the samples exhibit large net optical gain. Dramatic enhancement of photorefractive performance was obtained after adding a small amount of trapping molecules, especially, the net gain of for the sample containing only 0.05% **M1** reached 235 cm^{-1} under a field of 35 V/cm, which is among the largest to date at such a low field.[10] It can be noted that a maximum gain coefficient can be obtained when the concentration of **M1** is around 0.05%. Further increase in concentration of **M1** leads to a significant decrease in photorefractive gain.

In order to gather further information about the amplitude of the refractive index grating, degenerated four wave mixing (DFWM) experiments were carried out to compare the diffraction efficiencies. The maximum diffraction efficiencies (%) and related field strengths (V/μm) were determined to be 67.2% at 26 V/μm, 69.1 at 26, 77.5 at 23, 75.2 at 24.5 and 35.4 at 30.7 in the through pure **M01**; (b) trapped by core of **M1**; (c) de-trapping; (d) transport through **M1**. order of **M1** concentration increase for all the five materials (Figure 10). Again, the sample containing only 0.05% **M1** shows the highest diffraction efficiency at the lowest field.

From the above results, we can note that the same trend exists in terms of both optical gain and diffraction efficiency: 0.5% < 0 < 0.01% < 0.1% < 0.05%. Our explanation is as follows: for pure **M01**, when the charge carriers (electrons) are generated by illumination of laser beams, they will be trapped by some defects introduced when films are made to realize the space-charge field necessary for refractive-index modulation, but the trap density could be very low for pure monolithic material; when **M1,** which incorporates the more electron deficient core (**M**) is introduced, the generated electrons will be quickly trapped by the electronically more favorable cores (Figure 7), and the space-charge field will be built up instantly and more efficiently. The more traps, the stronger the built-up space-charge field and also the better the PR properties. However further increase of the concentration of **M1** will create a new electron-transporting pathway and the effective trapped charges will be reduced. Thus, the magnitude of the internal field will be decreased, so will the PR performances. According to the above observation, the optimum addition of **M1** is between 0.05-0.1% wt of **M01**, which corresponds to only one **M1** molecule per 5000 (3200-6400) **M01** molecules. Using the relationship $\rho \sim n^{-1/3}$, where ρ in the inter-trapping center distance (cm), n is the trap density (cm^{-3}),[11] we can estimate that distance is about 15 (13-17) nm for the optimum addition of **M1** (0.05-0.1% wt with **M01**).

References.

(1) Reviews: (a) Moerner, W. E.; Silence, S. M. Chem. Rev. 1994, 94, 127. (b) Yu, L.; Chan, W. K.; Peng, Z. H.; Gharavi, A. Acc. Chem. Res. 1996, 29, 13. (c) Zhang, Y.; Burzynski, R.; Ghosal, S.; Casstevens, M. K. Adv. Mater. 1996, 8, 111.

(2) Solymar, L.; Webb, D. J.; Grunnet-Jepsen, A. The Physics and Applications of Photorefractive Materials Clarendon Press, Oxford, 1996.

(3) (a) Moerner, W. E.; Grunnet-Jepsen, A.; Thompson, C. L. Annu. Rev. Mater. Sci. 1997, 27, 585. (b) Yu, L. J. Polym. Sci. Part A: Polym. Chem. 2001, 39, 2557. (c) Würthner, F.; Wortmann, R.; Meerholz, K. ChemPhysChem 2002, 3, 17.

(4) (a) Wang, Q.; Wang, L.; Yu, L. Macromol. Rapid Commun. 2000, 21, 723. (b) Zilker, S.J. ChemPhysChem 2000, 1, 72.
(5) Malliaras, G. G.; Krasnikov, V. V.; Bolink, H. J.; Hadziioannou, G. Appl. Phys. Lett. 1995, 66, 1038
(6) Grunnet-Jepsen, A.; Wright, D.; Smith, B.; Bratcher, M.S.; DeClue, M.S.; Siegel, J.S.; Moerner, W.E. Chem.Phys.Lett. 1998, 291, 553
(7) Wang, L.; Ng, M. K.; Yu, L. Appl. Phys. Lett. 2001, 78, 700.
(8). You, W.; Hou, Z.; Yu, L., Appl. Phy. Lett., Submitted.
(9) Tg was determined to be 28°C for M0 and 96°C for M1, respectively.
(10) Aiello, I.; Dattilo, D.; Ghedini, M.; Golemme, A. J. Am. Chem. Soc. 2001, 123, 5598.
(11) Mort, J.; Pfister, G. In Electronic Properties of Polymers; Mort, J., Pfister, G., Eds; John-Wiley and Sons, Inc. 1982; pp 215-265.

4. Different response of Electron Trap in a Monolithic Materials.

The above monolithic materials offer opportunities to fine-tune PR properties through modification of the molecular structure.[5] We also observed a dramatic improvement of PR performances in one monolithic material based on compound **M01** when appropriate trapping molecules were intentionally added to capture the charge carriers. Even though these are simplified materials that can be purified very carefully, unexpected results can be obtained, which lead us to a deeper appreciation about the complexity of the photorefractive phenomenon in organic materials. W found surprising results of the effect of the trapping molecule on PR properties of two related materials **M01** and **M01**

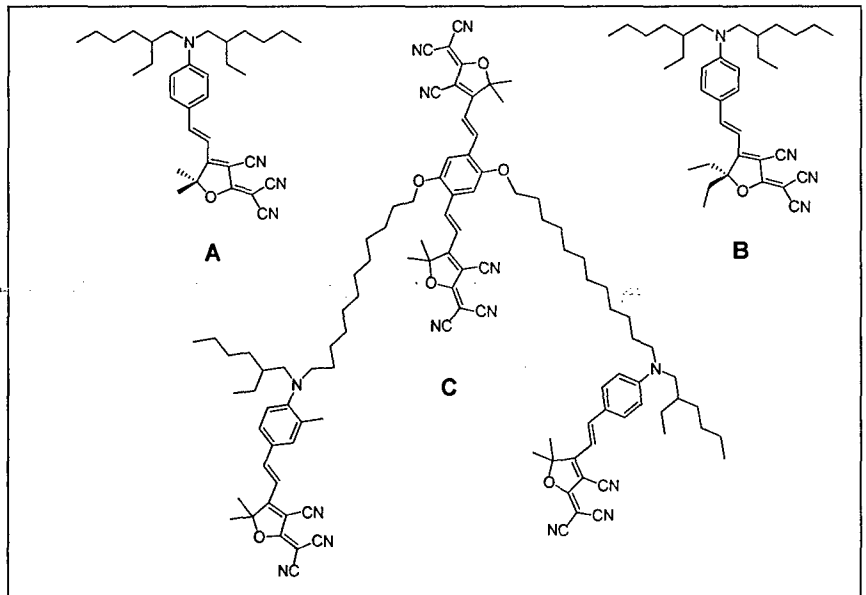

Figure 11. Molecular structures of materials studied.

The molecular structures of materials are shown in Figure 11. The films for our experiments were fabricated by heating the materials near the melting points and then sandwiching them between two glass substrates coated with indium tin oxide (ITO). The thickness of the sample was

pre-determined with the polymer film spacer. The absorption coefficients of the samples were measured with a UV-visible spectrophotometer (Shimadzu UV-2401PC). The change of the side chain does not affect conjugation length and has little influence on the absorption peak, 595.5 nm for **A** and 593.5 nm for **B**. The resulting films after doping with **C** are amorphous, as confirmed with wide-angle X-ray diffraction experiments. The refractive index of the film was determined at 780nm with the prism-coupling method (Metricon model 2010 prism coupler).

PR gain and diffraction efficiency were determined at 25 °C with two-beam coupling and degenerated four-wave mixing experiments, respectively. As a standard method for two-beam coupling, the two *p*-polarized laser beams, with intensities of $I_1(0)$ and $I_2(0)$, were overlapped in the film to write the grating. The sample was tilted at 53°, with an external intersection angle of 18°. The intensities behind the sample, $I_1(L)$ and $I_2(L)$, were measured as a function of the applied field. The incident two-beam intensities were equal at 568 mW/cm^2. The gain coefficient was calculated by using the expression,

$$\Gamma = [\ln(\gamma\beta) - \ln(\beta + 1 - \gamma)]/L \qquad (1)$$

where L is the optical path length for beam I_1, β is the ratio of the two input beam intensities, $\beta = I_2(0)/I_1(0)$, γ is the beam coupling ratio defined as the ratio of intensities of $I_1(L)$ with and without the presence of I_2, $\gamma = I_1(L)(I_2 \neq 0)/I_1(L)(I_2 = 0)$.

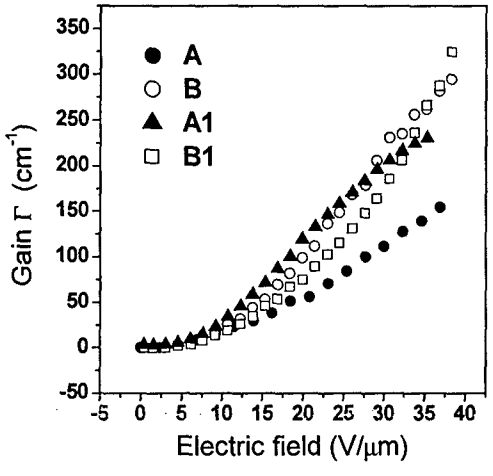

FIG. 12. Optical gain coefficients as a function of external fields of four samples **A, A1, B** and **B1**.

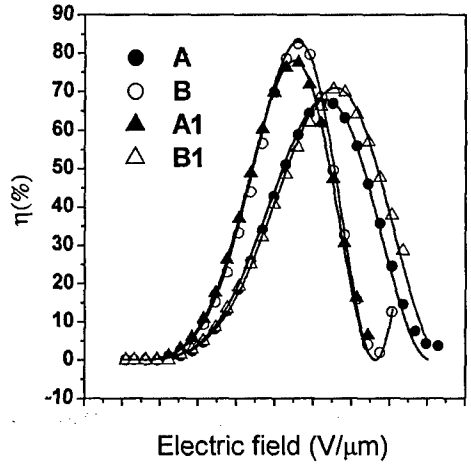

FIG. 13. Diffraction efficiency as a function of external fields of four samples **A, A1, B** and **B1**.

The dependence of the gain coefficients on the external field for the samples is shown in Figure 12. The net gain of the sample **A1** (**A** containing 0.05 wt% **C**) reached 235cm^{-1} (35 V/μm) and almost doubled the value (120cm^{-1}) for the pure sample **A** at the same electric field. But the optical gain coefficient of the sample **B1** (**B** containing 0.05 wt% **C**) was reduced at a low external field and became almost the same as that of the sample **B**, about 250cm^{-1} at 35 V/μm and then exceeded that of **B** when the field was increased above 35 V/μm.

Degenerated four-wave mixing experiments were performed with two *s*-polarized beams at an equal intensity of 568 mW/cm^2, overlapped in the film to write the grating. A weak *p*-polarized

reading beam with an intensity of 12.5 mW/cm^2 was counter-propagated to one of the writing beams to detect the process of grating buildup. The normal of the surface was tilted 53° with respect to the symmetric axis of the two intersected beams and the external crossed angle of the two beams was 18°. The diffraction efficiency is defined as the ratio between the intensity of the diffracted beam and the transmitted beam intensity in the absence of the two writing beams.

The field dependence of diffraction efficiencies for different materials is shown in Figure 13. Sample **A1** showed a larger maximum diffraction efficiency and its $E_{\pi/2}$ value (the applied fields at the maximum diffractions) shifted towards the lower field at 23 V/μm close to the value of sample **B**. However, the diffraction efficiency of the sample **B1** showed lower maximum diffraction efficiency and its $E_{\pi/2}$ value shifted to a higher field at 26 V/μm, close to the value of sample **A**.

The superior properties of **B** over **A** were attributed to the weakened intermolecular interaction due to the ethyl group that is one carbon longer than methyl groups in **A**.[5] The improvement of the PR properties by doping **C** into **A** was reasonably explained by assuming that molecule **C**, which exhibits a lower LUMO energy level than **A**, serves as internal traps for electrons.[10] Several experimental results support that assumption. The puzzling point is that although both molecules **A** and **B** exhibit similar energy levels as determined by cyclic voltammetry experiments, the effect of the trapping molecule **C** on their PR effect seems to be opposite.

To understand the inherent difference and reveal the underlying mechanism, the carrier mobility of different samples was measured as a function of temperature. The carrier mobility μ was determined from the conventional time-of–flight method from the expression, $\mu=L^2/\tau V$, where L is the thickness of the charge transport layer, τ is the transit time of the charge carriers, and V is the voltage across the sample layer. The typical transient photocurrent showed dispersed characteristics due to the randomized dipole electric fields in the materials. Both hole and electron transient photocurrents were observed, indicating that our materials exhibit bipolar transport. The transient times were determined in double log plots of transient currents as a function of time. Figures 14a and 14b are the Arrhenius plots of hole and electron mobility of the samples and the data were collected at 30 V/μm. The calculated values of activation energy were listed in Table 2.

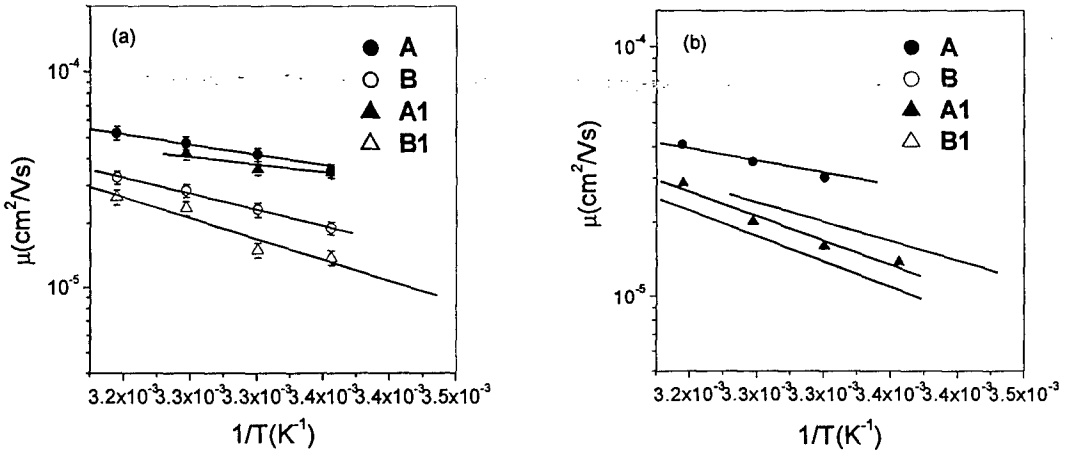

FIG. 14. Arrhenius plots of hole (a) and electron (b) mobility of four samples **A, A1, B** and **B1** at 30 V/μm.

TABLE 2. Summary of the physical properties of four materials.

	α (cm^{-1})	HOMO (eV)	LUMO (eV)	$E_{\pi/2}$ (V/μm)	E_{ah} (eV)	E_{ae} (eV)	μ_h ($\times10^{-5}cm^2/Vs$) [25°C]	μ_e ($\times10^{-5}cm^2/Vs$) [25°C]
A	1.7	-5.289	-3.588	26	0.189	0.192	3.49	3.02
A1	2.5			23	0.143	0.311	3.42	1.6
B	6.2	-5.303	-3.567	23	0.296	0.391	1.89	1.37
B1	7.3			26	0.385	0.408	1.38	1.12
C		-5.278	-4.033					

Results in Figure 14b show that compound **C** served as the electron trap when it was doped into **A**, noticeably reducing the electron mobility. This viewpoint was reinforced by the experimental value of electron activation energy (E_{ae}) of **A1**, which increased about 0.12 eV when compared with that of **A**. Moreover, the electron mobility of **A1** decreased greatly by $1.42\times10^{-5}cm^2/Vs$ at 25 °C when compared with that of **A** (3.02×10^{-5} cm^2/Vs at 25 °C). This trend is in accordance with the LUMO energy difference between **A** and **C** ($\Delta E_{LUMO} = 0.445$ eV), indicating compound **C** is an effective electron trapper. The results imply that the trapped electrons are the main source of increased internal space-charge field. The charge mobility of both hole and electron in material **B** was smaller than those of **A** and the activation energies of charge transport increased. It seems that the ethyl side chains at the electron withdrawing part increased the energy barrier for the charge transport. However, they affected much more on electron activation energy ($\Delta E_{ae}=E_{ae[B]}-E_{ae[A]}=0.199$ eV) than on hole activation energy ($\Delta E_{ah}=E_{ah[B]}-E_{ah[A]}=0.107$ eV), though the HOMO and LUMO energy levels for **A** and **B** are almost identical. After doping **C** into **B**, the mobility of both electron and hole diminished further, but the difference of carriers' mobility of **B1** decreased ($\Delta\mu=\mu_h-\mu_e=0.26\times10^{-5}cm^2/Vs$ at 25 °C) compared with that of **B** ($\Delta\mu=\mu_h-\mu_e=0.52\times10^{-5}$ cm^2/Vs at 25 °C).

These results present a curious case that a very subtle change in molecular structures leads to a dramatic effect in photorefractive performances. A possible explanation is as follows. The longer alky chain in molecule **B** introduces an additional energy barrier for charge transportation, which might stem from the increased intermolecular distance and the weakened interaction between adjacent molecules. Due to low glass transition temperature, the reorientational enhancement in material **B** (Tg=20.9 °C) is better than material **A** (Tg=25.7 °C). Photorefractive materials from molecule **B** have better performances with larger gain and smaller $E_{\pi/2}$ value. When the molecule **C** was doped into **A**, it behaved as an effective electron trapping center as we stated above, which greatly enhanced its PR performances; gain increased and $E_{\pi/2}$ value reduced. However, when **C** was doped into **B**, it did not play the sole role of effective electron trap as we expected from the viewpoint of energy levels and it became an effective trapping center for both electrons and holes instead. It is possible that under an external field, the two dipoles in molecule **C** will be aligned somewhat parallel to each other and the core moiety will not be reoriented. Molecule **B** is then more difficult to insert into the **U**-shaped molecules than **A** due to the structural difference between **B** and **C**, and molecule **C** will **disrupt** the packing and block the charge transfer pathway. Both the trapped holes and electrons will experience higher activation energy (in Table 2). Molecule **C** virtually functions as a universal trap for both electrons and holes instead of serving as the electron

traps in the case of **A1**. The more effective trapping of both charge carriers causes reduction in the effective space charge field due to cancellation. Therefore, the PR performances of **B1** diminished with reduced optical gain reduced and increased $E_{\pi/2}$ value.

These results are consistent with the bipolar two-trap model. The materials we studied have both hole and electron carriers. A signature of bipolar transport was also observed in our four-wave mixing experiments in which the temporal diffraction minima upon erasure were observed due to the competition of hole and electron grating.[11] The bipolar two-trap model predicts an expression for the steady space-charge field (E_{SC}) which is related to trap-limited hole (E_{qA}) and electron (E_{qD}) space-charge field. Under the condition of $E_0 >> E_D$, E_{SC} can be expressed as

$$E_{SC} = \frac{(E_{qA} - E_{qD})(E_0 - jE_D)}{(E_{qA} - E_{qD}) + (E_0 + jE_D)} \qquad (2)$$

where E_0 is the external field and E_D is the diffusion field. For PR materials, the appropriate trap density must be present in order to build up the efficient space-charge field. Based on the experimental results, if the trap density is too low or too high, we can only observe fast mobility and a small space-charge field.[10] For our bipolar-trap materials, the efficient PR performances are related to the net trap-limited space charge field (E_{qA}- E_{qD}), not E_{qA} or E_{qD} solely.

The net trap-limited space charge field is closely related to the difference of mobility between electrons and holes. Therefore, according to the aforementioned charge mobility difference, the PR performances of **A1** could be enhanced when compared with **A**, while the PR performances of **B1** were not improved when compared with **B**. The low mobility and high activation energy should lead to the degraded PR performances for **B** and **B1** compared with **A**, but their lower glass transition temperatures benefit their PR performance improvement due to the "orientational enhancement" effect.[12]

The differences of the net space-charge field among our samples were also observed in degenerate four-wave mixing experiments (Figure 13). According to Kogelnik's theory,[13] under the same experimental conditions, if we assume the contribution from electro-optic and orientational enhancement effects is almost the same before and after doping **C** into **A** or **B**, the only factor to influence the $E_{\pi/2}$ value is the net space-charge field. The shift of $E_{\pi/2}$ values for different samples is in accordance with our explanation on net space-charge field based on the mobility and activation energy.

Another interesting observation is that the optical gain of material **B1** surpasses that of material **B** when the external field is larger than 37 V/μm. This can be understood by considering the fact that the holes have activation energy of 0.385 eV and the electrons of 0.408 eV. When the external field is large enough to overcome the activation energy of holes, the net density of electrons trapped will be enhanced and the PR performances will surpass that of pure **B** where the activation energy of electrons is about 0.391 eV. In that field range, molecule **C** plays effective electron trapper even in materials **B1.**

References:

[1] W. E. Moerner and S. M. Silence, Chem. Rev. **94**, 127 (1994).
[2] W E. Moerner, A. Grunnet-Jepsen, and C. L. Thompson, Annu. Rev. Mater. Sci. **27**, 585 (1997).
[3] S. J. Zilker, ChemPhysChem **1**, 73 (2000).
[4] L. Wang, M.-K. Ng, and L. Yu, Appl. Phys. Lett. **78**, 700 (2001).
[5] Z. Hou, W. You and L. Yu, Appl. Phys. Lett. **82**, 3385 (2003).
[6] U. Gubler, M. He, D.Wright, Y. Roh, R. Twieg, and W. E. Moerner, Adv. Mater. **14**, 313 (2002).
[7] O. Ostroverkhova, D. Wright, U. Gubler, W. E. Moerner, M. He, A. Sastre-Santos, and R. J. Twieg, Adv. Funct. Mater. **12**, 621 (2002).
[8] O. Ostroverkhova, W. E. Moerner, M. He, and R. J. Twieg, Appl. Phys. Lett. **82**, 3602 (2003).

[9] J. Sohn, J. Hwang, S. Y. Park, J.-K. Lee, J.-H. Lee, J.-S. Jang, G. J. Lee, B. Zhang, and Q. Gong, Appl. Phys. Lett. 77, 1422 (2000).
[10] W. You, Z. Hou, and L. Yu, Adv. Mater. **16**, 356 (2004).
[11] L. Wang, M.-K. Ng, and L. Yu, Phys. Rev. B. **62,** 4973 (2000).
[12] A. Grunnet-Jepsen, C. L. Thompson, and W. E. Moerner, J. Opt. Soc. Am. B **15**, 905(1998).
[13] H. Kogelnik, Bell Syst. Tech. J. **48**, 2909 (1969).

5. Pronounced Photorefractive Effect at Wavelength over 1000 nm in Monolithic Organic Materials

Most of organic photorefractive materials only function at wavelengths below 800 nm. Considering the potential applications, such as real-time optical data processing at a wavelength ranging from 1.3 to 1.5 μm commonly used in optical communication,[3] photorefractive materials with high performance at these wavelengths are of great interest. Currently, there are only a limited number of hybrid materials found to be sensitive at wavelength over 1000 nm, either by new polymer composites[4] or by using the nanocrystals as the sensitizers.[5]

We found that extension of the conjugation length of the chromophores caused the bathochromic shift of the absorption and rendered the new materials pronounced photorefractive effects at a wavelength of 1064 nm.

The structures of the molecules are shown in Figure 1 and their synthetic procedures are similar to the reported procedure.[8,9] The two hexyl groups were introduced to the electron-withdrawing parts so that low glass transition (T_g) temperatures of both materials made from **T6** and **B6** can be obtained. Indeed, DSC experimental results indicated T_g values of 22.5 °C for **T6** and 19 °C for **B6**, respectively. The films for our experiments were fabricated by heating the materials near the melting points and then sandwiching them between two glass substrates coated with indium tin oxide (ITO). The thickness of the sample was pre-determined with the polymer film spacer.

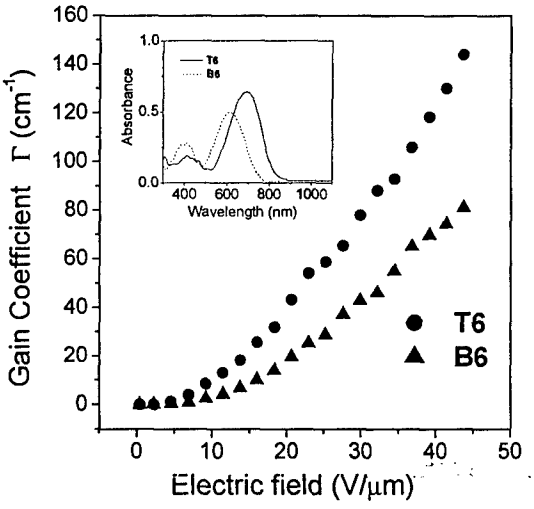

FIG. 15. Dependence of the gain coefficients Γ from 2BC on the applied field, Inset: UV–Vis absorption spectra of **T6** and **B6** measured in chloroform solution (1×10^{-5} M) at 25 °C.

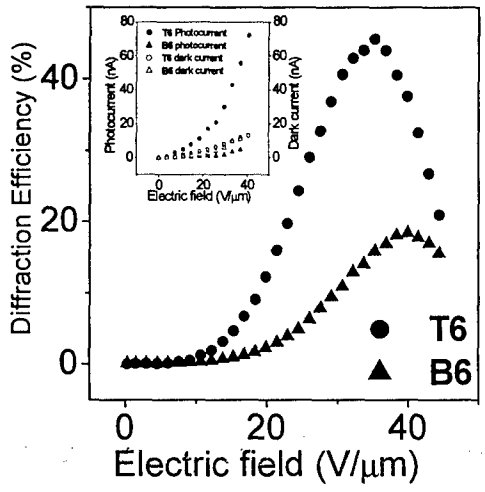

FIG. 16. Applied field dependence of the diffraction efficiency from DFWM experiment. Inset: Dependence of the photocurrent and dark current on the applied field at 1064 nm.

The UV-Vis spectra of the two molecules are shown in the inset of Figure 2. The major absorption bands for **T6** and **B6** appear around 689 nm and 613 nm, respectively. The photosensitivity at wavelength over 1000 nm (e.g. 1064nm) was observed due to the tailing into longer wavelength of the absorption spectra. Cyclic voltammetry (CV) studies revealed three oxidation potentials for **T6** due to the presence of electron-rich nitrogen and thiophene moieties while only one oxidation process can be observed for **B6**. Both compounds showed only one reduction process. Based on the measured redox potentials, the HOMO and LUMO energy levels were estimated.[10] The HOMO energy level of **T6** is around – 4.94 eV, which is slightly higher than that of **B6** (– 4.96 ev); the LUMO energy level of **T6** (– 3.74 eV) is slightly lower than that of **B6** (– 3.72 eV).

Two-beam coupling (2BC) experiments were performed at 25 °C by intersecting two split p-polarized laser beams (Intellite diode laser, 1064nm) with equal intensity (2×230 mW/cm^2) in the film with an external cross-angle of 20° to generate the refractive index grating. The film normal was tilted an angle of 53° with respect to the symmetric axis of the two writing beams to provide a nonzero projection of the grating wave vector along the poling axis. The transmitted intensities of the two beams were monitored by two calibrated diode detectors. A pronounced PR effect for both materials at 1064 nm was observed as evidenced by a clear asymmetric energy transfer between the two beams As indicated in Figure 15, the gain coefficients (Γ) for both materials increase as the external field increases, but the material based on molecule **T6** consistently shows larger optical gain than the benzene-based molecule **B6**. For example, a high gain coefficient of 144.1 cm^{-1} at a relatively low applied field of 43.7 V/μm can be obtained for **T6**, but only 81.3 cm^{-1} for **B6** at the same field. Considering the absorption coefficients (α) for **T6** and **B6** are 5.00 and 2.13 cm^{-1},

respectively, both molecules exhibit net optical gain of 139.1 and 79.1 cm^{-1} at the field of 43.7 V/μm, respectively.

Degenerated four wave mixing (DFWM) experiments were also carried out at 25 °C to gain more insightful information about the amplitude of the refractive index grating. Two s-polarized laser beams (1064 nm) of equal intensity (2×230 mW/cm^2) intersected in the film to write the index grating, and a weak p-polarized beam (probe beam, 7.5 mW/cm^2) counter-propagating to one of the writing beams was used to read the index grating formed in the material. The diffracted light intensity of the probe beam was detected by a photodiode and subsequently amplified with a lock-in amplifier. The diffraction efficiency η was calculated as the ratio of the intensity of the diffracted beam to the transmitted beam intensity in the absence of the two writing beams. The maximum diffraction efficiencies were determined to be 45.6% at 35.3 V/μm, 18.4% at 40 V/μm for **T6** and **B6**, respectively (Figure 16). Once again, **T6** shows superior properties over **B6** in terms of diffraction efficiency.

Since both materials form amorphous solid with low glass transition temperatures, it can be assumed that the intermolecular interaction in both materials is similar. The CV studies indicated a very similar electrochemical behavior. There are two factors that are responsible for the difference in their PR performances, namely, absorption coefficients and dipole moments. According to the figure of merit (FOM) for low T_g organic PR materials[11]

$$F = \frac{1}{M}\left(9\mu\beta + \frac{2\mu^2\Delta\alpha}{k_bT}\right) \qquad (1)$$

(where μ is the dipole moment, $\Delta\alpha$ the anisotropy of the linear polarizability, β the second-order polarizability, k_b the Boltzmann constant, T the temperature, and M the molar mass), maximizing the dipole moment would improve the PR performance. Theoretical calculation by using the optimized geometries at the HF/6-31G* level indicated dipole moments of 18.024 Debye for **T6** and 17.064 Debye for **B6**. Thus, **T6** should possess higher optical gain than **B6**.

However, the small difference in dipole moments alone cannot explain the magnitude of differences in optical gain. As mentioned above, the absorption coefficients (α) for **T6** are 5.00 cm^{-1}, more than double that of **B6** (2.13 cm^{-1}). Larger absorption coefficient helps **T6** generate more charge carriers. This is confirmed from photoconductivity measurements. The photoconductivity was measured using a DC technique at the wavelength of 1064 nm with an intensity of 16 mW/cm^2. The sample thickness was 27 μm. The data were recorded at the steady state and the net photocurrent was calculated as the difference between the total current in the presence of light and the dark current. It was shown that **T6** has a higher photoconductivity than **B6** upon illumination by the 1064 nm laser while their dark currents between T6 and B6 have only a slight difference (inset of Figure 15). At an external field of 33.3 V/μm, the observed net photocurrent for **T6** is 42.9 nA, but only 3.4 nA for **B6**. This difference must also be reflected in PR response times. The higher efficiency in photo-charge generation leads to faster internal field buildup and stronger internal charge field where the chromophores can reorient more quickly and easily in response to the integrated fields. From four wave-mixing experiments, it was observed that at an electric field of 31 V/μm, space charge field buildup time constant τ_1 is 1 s and dipole reorientation time constant τ_2 is 15.6 s for **T6**. At the same electric field, τ_1 is 1.5 s and τ_2 is 95.6 s for **B6**.

It was also found that **T6** is photosensitive at 1300 nm and a photocurrent of 0.8 nA was observed at 33.3 V/μm. A gain coefficient of 8.5 cm^{-1} (absorption coefficient is 1.86 at 1300 nm) was obtained for pristine sample at 43.7 V/μm.

Reference:

[1] W E. Moerner, A. Grunnet-Jepsen, and C. L. Thompson, Annu. Rev. Mater. Sci. **27**, 585 (1997).
[2] L. Yu, W. K. Chan, Z. H. Peng, and A. Gharavi, Acc. Chem. Res. **29**, 13 (1996).
[3] L. Solymar, D. J. Webb, and A. Grunnet-Jepsen, *The Physics and Applications of Photorefractive Materials* Clarendon Press, Oxford, (1996).
[4] A. Z. Kuzhelev, A. Dudelzak, P-P. Proulex, W. E. Douglas, L. D. Klapshina, and T. I. Lopatina, Proceedings of SPIE Organic Photonic Materials and Devices IV **4642**, 41 (2002).
[5] J. G. Winiarz, L. Zhang, J. Park, and P. N. Prasad, J. Phys. Chem. B **106**, 967 (2002).
[6] Z. Hou, W. You and L. Yu, Appl. Phys. Lett. **82**, 3385 (2003).
[7] O. Ostroverkhova, D. Wright, U. Gubler, W. E. Moerner, M. He, A. Sastre-Santos, and R. J. Twieg, Adv. Funct. Mater. **12**, 621 (2002).
[8] W. You, Z. Hou and L. Yu, Adv. Mater. **16**, 356 (2004).
[9] H. Saadeh, L. M. Wang, and L. P. Yu, Macromolecules, **33**, 1570, 2000.
[10] W. You, L. Wang, Q. Wang, and L. Yu, Macromolecules **35**, 4636 (2002).
[11] R. Wortmann, C. Poga, R. J. Twieg, C. Geletneky, C. R. Moylan, P. M. Lunquist, R. G. DeVoe, P. M. Cotts, H. Horn, J. E. Rice, D. M. Burland, J. Chem. Phys. **105**, 10637 (1996)

6. Fully Functionalized Photorefractive Polymer with Infrared Sensitivity Based on Novel Chromophores

In addition to the effort in monolithic PR materials, we also actively searched for fully functionalized PR materials. We synthesized a new (PR) polymer system. This work is motivated by our desire to prepare fully functionalized PR polymers with high performances. Several criteria were used in designing these polymers. Firstly, the PR polymers need to exhibit a large electro-optic coefficient so that the index modulation can be optimized. Secondly, it is ideal that the PR polymers possess low glass transition temperature so that the "orientational effect" of dipoles due to the photoinduced space charge field can be utilized to further enhance the PR performances. Low glass transition temperature also allows easy preparation of thick films for holographic studies. Thirdly, the polymer structures can be synthesized relatively easily under mild conditions.

In a PR polymer, the NLO chromophore plays a key role and a large E-O effect in the polymer is a necessary condition to achieve high PR performances. Recently our group, as well as other have found that chromophores bearing tri-cyano-dihydrofuran derivatives as the electron-withdrawing group exhibit a promising photorefractive effect in the form of monolithic materials.[12,13] It is of great interest to incorporate these chromophores into polymers because compared with the NLO chromophores which are not so stable small molecules, the resulting polymers could possess better stability in their amorphous state and the film forming could be easier for the polymers. To obtain low *Tg* polymers, different alkyl side chains will be introduced. Since these polymers are multifunctional materials made from incorporation of different functional monomers which are rather sensitive to reaction medium (esp. the chromophores), many traditional polymerization approaches are not compatible with these monomers. It was found that the palladium mediated Stille coupling reaction is mild enough to tolerate the NLO chromophore and yielded polymers with sizable molecular weight. These polymers demonstrated excellent PR properties and detailed physical studies disclosed insightful information about the structure-property correlation.

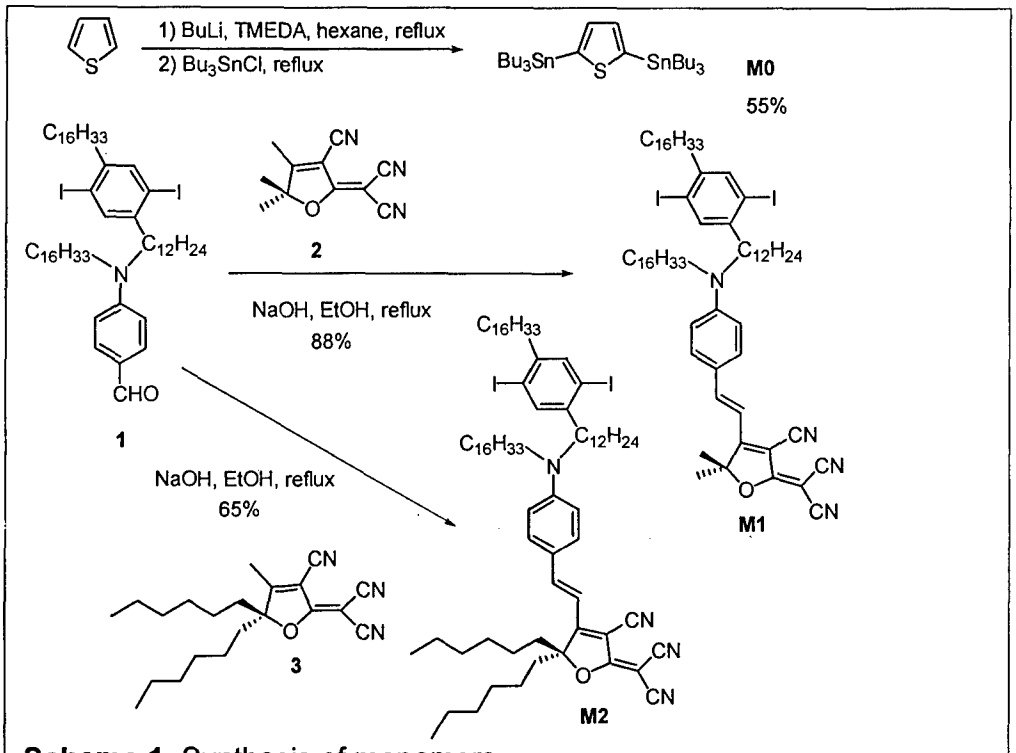

Scheme 1. Synthesis of monomers.

Results and Discussion:

Synthesis of Monomers and Polymers: The key components for the new chromophores are the electron-withdrawing moieties: tri-cyano-dihydrofuran derivatives (compound **2** and **3** in Scheme 1), which can undergo Knoevenagal condensation with substituted amino benzaldehyde **1** to afford the NLO chromphores/monomers **M1** and **M2.** As shown in Scheme 2, all the PR polymers were synthesized with high yields by palladium-catalyzed Stille polycondensation using $Pd(PPh_3)_2Cl_2$ as the catalyst and THF as the solvent.[14] Longer alkyl chains were used not only for the enhancement of the solubility, but also to lower the glass transition temperature of the resulting polymers. Based on the "Orientational Enhancement Effect",[15] lowering the T_g of the PR polymer could allow the chromophores to re-orient in response to the combined internal and external fields, and greatly improve the magnitude of the refractive index grating. Polymers **P1** and **P2** were synthesized from the corresponding monomers **M1** and **M2** with di(tributyltin) thiophene **M0**, respectively. The polymer **P3** is obtained from another monomer (dihexadecyl-diiodobenzene) together with **M1** in the ratio of 70:30. This polymer was synthesized in order to test our hypothesis that dilution of chromophores could weaken the intermolecular interaction between adjacent chrompophores and help to shorten the re-orientation time in response to the existing field. GPC measurement in THF with a polystyrene standard indicated the relative number averaged molecular weight (M_n) and the polydispersity (*PDI*) of all three polymers (**P1**: *Mn.*: 12400, *PDI*: 2.30; **P2**: *Mn.*: 15000, *PDI*: 2.08; **P3**: *Mn.*: 9000, *PDI*: 1.67). Differential scanning calorimetry (DSC) studies indicate that glass transition temperatures for **P1**, **P2** and **P3**, are around 20.1, 5.6, and 1.3°C, respectively. All the glass transition temperatures are lower than room temperature, as expected.

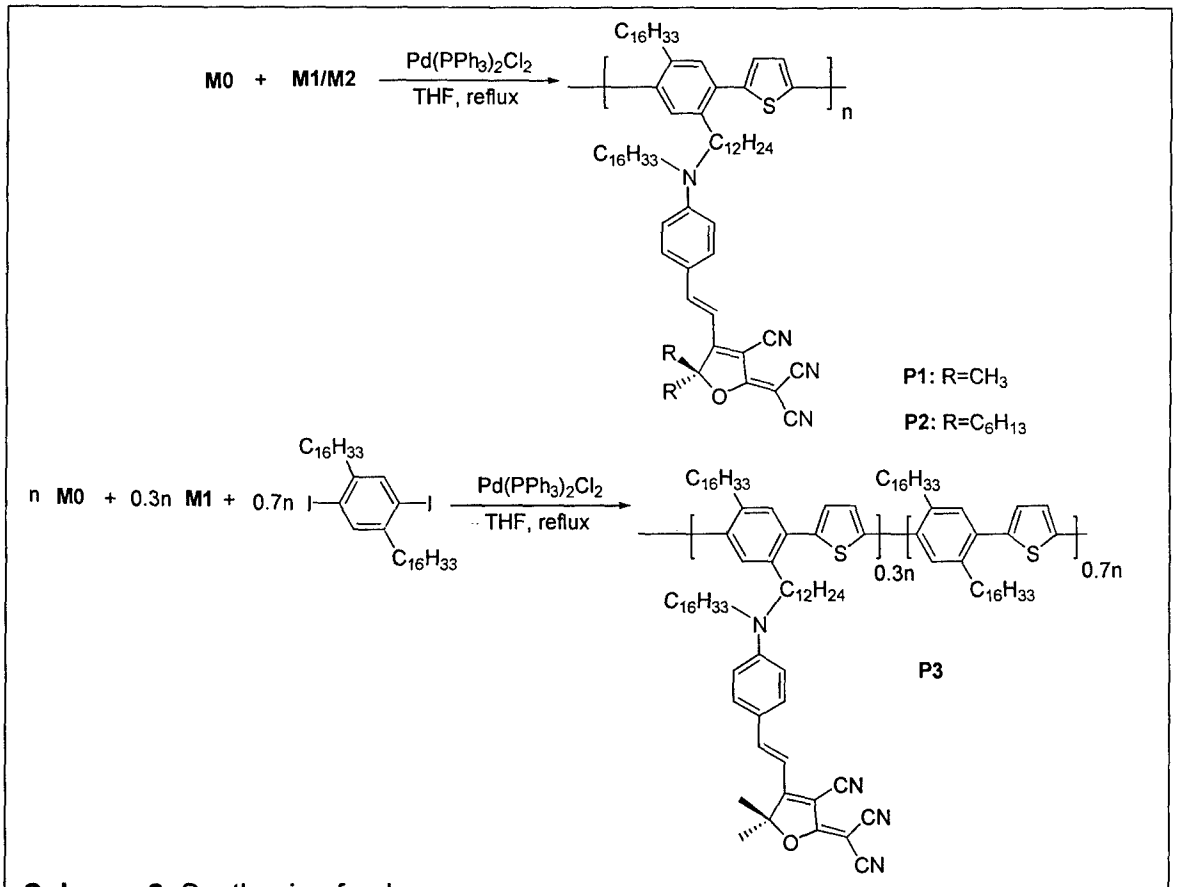

Scheme 2. Synthesis of polymers.

Optical Properties: The electronic absorption spectra of the monomers, **M1** and **M2**, and polymers, **P1**, **P2** and **P3**, were shown in Figure 17. Monomers **M1** and **M2** exhibit maximum absorptions at 592nm and 589nm, respectively, which also dominate the absorptions of the corresponding polymers, as listed in Table 3. The refractive indexes at 780nm for **P1, P2and P3** (in Table 4) were determined with the prism-coupling method (Metricon model 2010 prism coupler).

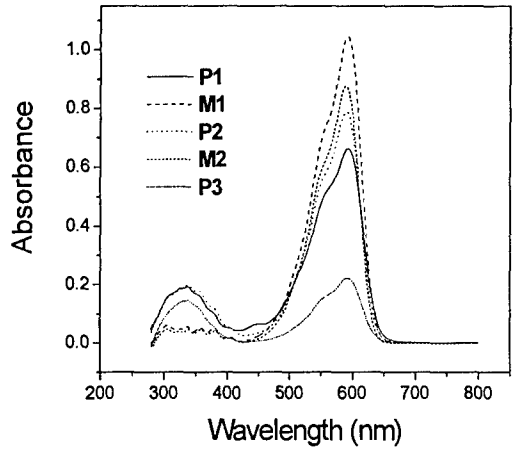

Figure 17. UV–vis absorption spectra of **M1**, **M2** and **P1**, **P2**, **P3** measured in chloroform solution (1×10^{-5}M) at 25 °C.

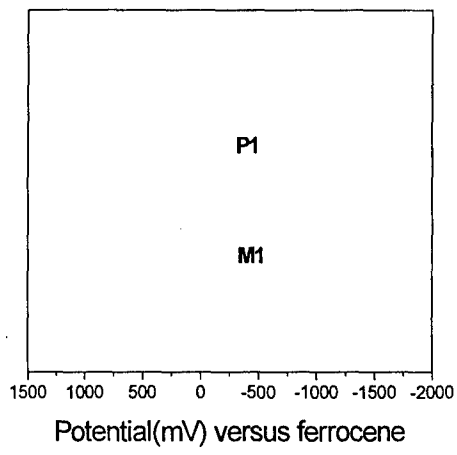

Figure 18. Cyclic voltammograms of monomer **M1** and polymer **P1** measured in 0.1 M Bu_4NPF_6 (supporting electrolyte) in methylene chloride at 25 °C and a scan rate of 25mV/s.

Table 3. Redox potentials and energy level for **M1**, **M2** and **P1**, **P2**, **P3**.

	E_{ox} (V)[b]	E_{red} (V)[b]	E_{ox}^{onset} (V)	E_{re}^{onset} (V)	E_{HOMO} (eV)	E_{LUMO} (eV)	E_{gap} (eV)
M1	0.54	-1.35	0.46	-1.25	-5.26	-3.55	1.71
M2	0.55	-1.30	0.47	-1.28	-5.27	-3.52	1.75
P1	0.55 0.79[c]	-1.36	0.46	-1.16	-5.26	-3.64	1.62
P2	0.57 0.78[c]	-1.29	0.49	-1.18	-5.29	-3.62	1.67
P3	0.56	NA[d]	0.48	NA	-5.28	NA	NA

[a] All potentials were calibrated with ferrocene/ferrocenium (Fc/Fc^+) couple.
[b] reported as $E_{1/2}$ values taken as the average of the anodic and cathodic peak potentials vs Fc/Fc^+.
[c] 2nd oxidation potential.
[d] no apparent peak observed clearly.

Redox Properties: The study of the redox properties of the monomers **M1** and **M2**, polymers **P1**, **P2** and **P3** were implemented by cyclic voltammetry (CV). Under the assumption that the energy level of ferrocene/ferrocenium is 4.8 eV below vacuum, the LUMO and HOMO energies levels

could be calculated according to $E_{HOMO} = -(E_{ox}^{onset} + 4.8)eV$, and $E_{LUMO} = -(E_{re}^{onset} + 4.8)eV$.[10] As indicated in Figure 18, Compound **M1** undergoes one-electron oxidation process, ascribable to the facile removal of an electron from the electron-rich amino moiety. The oxidation potential (E_{ox}) for **M1** is about 0.54 V (vs. Fc/Fc^+), which is almost the same as the first oxidation potential of polymer **P1** (0.55 V), while the second oxidation peak of **P1** can be barely observed at 0.79 V (vs. Fc/Fc^+), due to high order oxidation potential from the electron-rich backbone. Only one irreversible peak can be observed at –1.35 V (vs. Fc/Fc^+) for **M1**, identical to the reversible peak for polymer **P1** at –1.36 V (vs. Fc/Fc^+). The onset oxidation potential and the reduction potential for **M1**, at 0.46 V and -1.25 V (vs. Fc/Fc^+), were used to deduce the energy levels of of **M1**. It was found that the HOMO and LUMO energies for **M1** are –5.26 eV and –3.55 eV (vs. vacuum), respectively. Similar analysis was applied to all other materials and the results are summarized in Table 3.

Photoconductivity and Mobility: The photoconductivity and mobility measurements provide insightful information about the structure/property relationship. It was found that the photoconductivity measured at 780nm for **P1** is slightly larger than that of **P2** (0.072ps/cm vs. 0.065ps/cm), but much larger than that of **P3** (0.025ps/cm). This is because the concentration of the chromophores in **P1** is higher, which also serve as the photosensitizers and determine the amount of photogenerated charges. Bipolar (hole and electron) carriers were observed in these materials by the mobility measurement (time of flight (TOF) experiments) as we reported before with a similar system.[16] The bipolar transport is also confirmed in the time-dependent diffraction efficiency experiment (Figure 18). Both hole and electron mobility of **P1** are larger than those of **P2** since the close proximity of the chromophores in **P1** rendered by less bulky groups (methyl groups) might help charge carriers "hop" between adjacent chromophores.

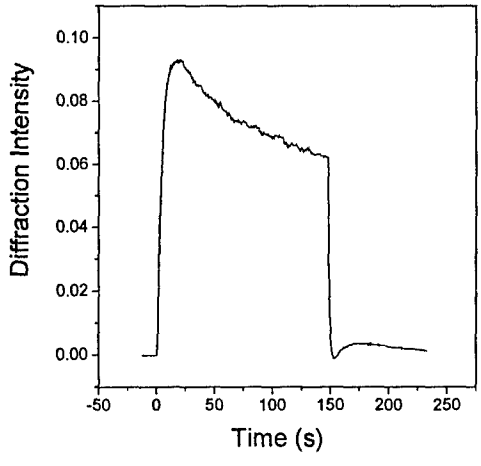

Figure 19. Diffraction efficiency as a function of time of polymer **P2** at an applied field of 31 V/μm. The writing beams are turned on at t=0, and one of the writing beans is blocked at t=150s.

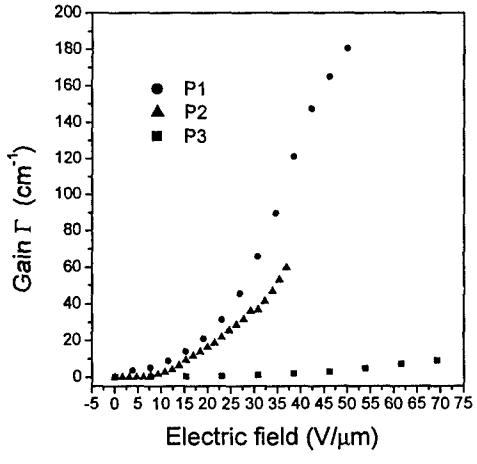

Figure 20. Optical gain coefficients of polymers **P1, P2,** and **P3** as a function of applied field.

Photorefractive Properties: In our previously reported PR polymeric systems and other fully functionalized PR polymers, photosensitizers such as metal-containing macrocycles, 2,4,7-trinitro-9-flurenone (TNF) or fullerene (C_{60}) are needed for charge generation. Polymers reported

here have been shown to be photoconductive due to the incorporation of the novel chromophores in the absence of any other photosensitizers. The unequivocal evidence for their PR nature was provided by two-beam coupling (2BC) experiments where two coherent laser beams with equal intensity (780nm, *p*-polarized, 2×948mW/cm^2) were intersected inside the thick polymer films. The asymmetric energy transfer between the two beams was clearly observed due to the phase shift between the incident light intensity and the refractive index modulation. The optical gain coefficient (Γ) was calculated using the following equation:

$$\Gamma = \frac{1}{L}\ln\left(\frac{\gamma\beta}{1+\beta-\gamma}\right) \qquad (1)$$

where β is the intensity ratio of the two incident writing beams, $\gamma = I_{probe}(I_{pump} \neq 0) / I_{probe}(I_{pump} = 0)$ is the ratio of intensities of the probe beam with or without the presence of the pump beam, and L is the optical path length of the beam with gain. As shown in Figure 20, the gain coefficients for all three polymers (**P1, P2** and **P3**) increase monotonically with the increment of the applied field. While **P1** shows the highest gain coefficient of 180 cm^{-1} at a relatively low field of 50 V/μm, **P2** exhibits a gain coefficient of 60 cm^{-1} at a field of 37 V/μm before the dielectric breakdown and **P3**, 8.8 cm^{-1} at 69 V/μm. Since the absorption coefficients (α) for **P1**, **P2** and **P3** are 24, 17.5 and 2.8 cm^{-1}, respectively, the net optical gain coefficient (Γ-α) are 158, 43 and 6cm^{-1} for **P1**, **P2** and **P3** at the fields mentioned. Thus, **P1** is the best among all three polymers in terms of both the gain coefficient and the net gain coefficient, which almost doubles the value of the highest gain of our recently reported polymers (83 cm^{-1} at a field of 60 V/μm, polymer **4** in ref 10).

To gain further insight into the PR nature of these polymers, degenerate four wave mixing (DFWM) experiments were performed, in which two *s*-polarized laser beams were used to write the PR grating and a weak *p*-polarized, counter-propagating beam served to read the index grating. The field dependence of the diffraction efficiencies for **P1** and **P2** is shown in Figure 21. Polymer **P1** consistently shows higher diffraction efficiency (η): 68% at a field of 46 V/μm, which is much higher than the functional polymers we reported before.[10] Due to the dielectric breakdown, the field applied to the film made with **P2** could not go beyond 37 V/μm, and a diffraction efficiency of 12% was observed at that field. For **P3**, no observable diffraction efficiency could be obtained.

These results can be interpreted based upon the figure of merit (FOM) for low T_g organic PR materials,[17]

$$F = \frac{1}{M}\ln\left(9\mu\beta + \frac{2\mu^2\Delta\alpha}{k_bT}\right) \qquad (2)$$

where μ is the dipole moment, $\Delta\alpha$ the anisotropy of the linear polarizability, β the second-order polarizability, k_b the Boltzmann constant, T the temperature, and M the molar mass. The elongation of alkyl group inevitably increases the molar mass (M in equation 2) and lead to the decrease of the FOM. Since the optical gain coefficient is a linear function of FOM, polymer **P2** exhibits a relatively lower gain than **P1**. For polymer **P3**, the low content (30%) of NLO chromophores is unfavorable to obtain a high optical gain. It is also conceivable that the electronic transport along the chromophore is diminished when the density of the chromophores is reduced, confirmed with experimental results from photoconductivity and mobility measurements (in Table 4). The above argument is reinforced by the observed trend of the diffraction efficiency.

Table 4. Typical physical properties of the PR polymers.

Compound	λ_{max} (nm) [$CHCl_3$]	α (cm^{-1})	n [780nm]	σ^a(ps/cm) [780nm]	T_g (°C)	$\mu_h{}^b$ (cm^2/V)	$\mu_e{}^b$ (cm^2/V)
P1	593	24	1.688	0.072	20.1	1.6×10^{-5}	2.6×10^{-5}
P2	590.5	17.5	1.679	0.065	5.6	4.8×10^{-5}	5.5×10^{-5}
P3	592.5	2.8	1.611	0.025	1.3	NA[c]	NA[c]

[a] measured at an applied field of 33 V/μm with intensity 175 mW/cm^2

[b] measured at an applied field of 33 V/μm with time of flight method at 532nm, experimental detail see reference 17.

[c] no detectable transit current was observed at the condition of b.

However, the lower glass transition temperature for **P2** seems to reduce the response time, measured by using DFWM and determined by fitting numerically the following quadratic biexponential function:[18]

$$\eta(t) = \eta_0 \left\{ 1 - \left[a \exp\left(\frac{-t}{\tau_1}\right) + (1-a)\exp\left(\frac{-t}{\tau_2}\right) \right] \right\}^2 \qquad (3)$$

where η is the time dependent diffraction efficiency, η_0 is the diffraction efficiency in the steady state, τ_1 and τ_2 are the fast and slow time constants respectively and a is a dimensionless weighting factor.

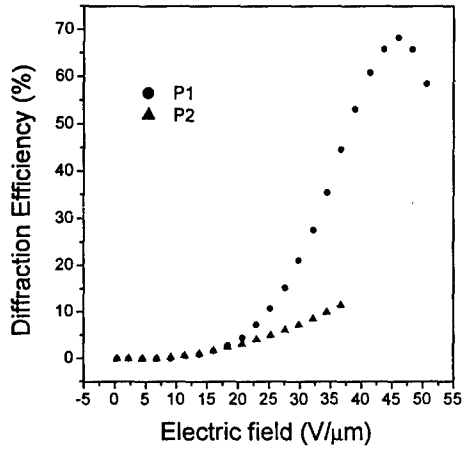

Figure 21. Diffraction efficiency of polymers **P1, P2**, and **P3** as a function of applied field.

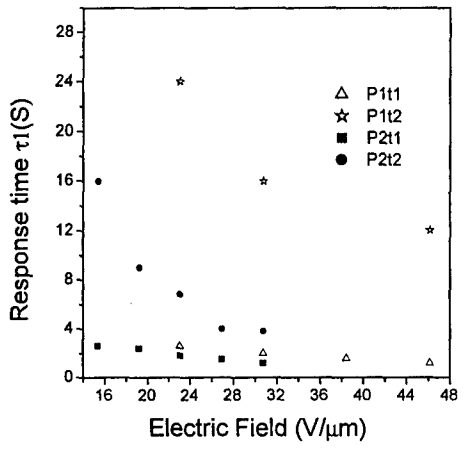

Figure 22. Response time constants of polymers **P1, P2** as a function of applied field.

The existence of two main processes in low T_g organic PR materials, the build up of the space charge field and the contribution of the orientation of the chromophores, justifies the use of

the biexponential equation. The temporal change of the space charge field could be related to the fast time constant τ_1; while the slow τ_2 indicates the reorientation of the chromophore in the combined fields. As indicated in Figure 22, the higher the field, the faster the response time constants. At the same electric field, both τ_1 and τ_2 for **P1** are smaller than those for **P2**. The fast time constant τ_1 does not vary too much for **P1** and **P2** (e.g. at external field of 31 V/μm, 2.0s for **P1** and 1.2s for **P2**) due to structural similarities between the two constructing chromophores (and also the polymers). The slight difference in τ_1 can be interpreted according to the differences in the charge carrier mobility (Table 4). The faster the mobility, the quicker the buildup of the internal electric field which results the smaller τ_1. However, for the slow time constant τ_2, the glass transition temperature starts to play a crucial role: at the same field of 31 V/μm, the polymer **P2** with a T_g of 5.6°C shows response time of 3.8s, but the **P1** with much higher T_g of 20.1°C shows a response time of 16s. Lower T_g means the chromophores gain more free volume at the room temperature to reorient in response to the integrated fields, resulting in a faster reorientation time.

Experimental Section:

General Methods. All chemicals were purchased from commercial suppliers and used as received unless otherwise specified. All reactions were carried out under a nitrogen atmosphere unless otherwise noted. Tetrahydrofuran (THF) was distilled over sodium and benzophenone. The ^{1}H-NMR spectra at 500 MHz and ^{13}C NMR spectra at 125 MHz were collected on Brüker DRX-500 spectrometer. UV/Vis spectra were recorded on a Shimadzu UV-2401PC spectrometer. Solution UV–vis spectra were measured as 1×10^{-5}M solutions in chloroform at 25°C. Thermal analyses were performed on Shimadzu DSC-60 and TGA-50 under nitrogen atmosphere at a heating rate of 5°C/min. Cyclic voltammetry was performed on a Bioanalytical Systems CA-50W with a three-electrode compartment cell (Bioanalytical Systems Inc.) equipped with a platinum disk as working electrode, a platinum wire as counterelectrode, and a $Ag/AgNO_3$ electrode as reference electrode. The supporting electrolyte used was tetrabutylammonium hexafluorophosphate (0.1 M in methylene chloride). The scan rate was adjusted to 25 mV/s. All potentials were calibrated with a ferrocene/ferrocenium (Fc/Fc+) couple. All reported $E_{1/2}$ values are taken as the average of the anodic and cathodic peak potentials. Mass spectrometry was provided by Hewlett Packard Agilent 1100 LCMSD. Elemental analyses were performed by Atlantic Microlab, Inc. Molecular weights and distributions were measured with a Waters RI and UV GPC system (Waters 410 Differential Refractometer and Waters 486 Tunable Absorbance Detector) with polystyrene as the standard and THF as the eluent. The films for two-beam coupling and four-wave mixing experiments were prepared by sandwiching the materials between two indium-tin oxide (ITO) covered glass substrates. Homogeneous film samples suitable for two-beam coupling and degenerate four-wave mixing experiments were prepared by sandwiching a slightly warmed material (~30-55 °C) between two indium–tin oxide (ITO)-coated glass substrates with thickness controlled by a polyimide spacer, affording film thickness of ~130 μm. Samples so prepared were also used for measurement of the absorption coefficients (α). Two-beam coupling experiments were performed using a diode laser (780nm, 50mW) as the light source. The two split *p*-polarized laser beams with equal intensity (2×948mW/cm^2) were intersected in the film with an external cross-angle of 18° to generate the refractive index grating. The film normal was tilted an angle of 53° with respect to the symmetric axis of the two writing beams to provide a nonzero projection of the grating wave vector along the poling axis. The transmitted intensities of the two beams were monitored by two calibrated diode detectors. Diffraction efficiency was measured by degenerate four-wave mixing (DFWM) experiment, in which two *s*-polarized laser beams (780nm) of equal intensity (2×948mW/cm^2) intersected in the film to write the index grating, and a weak *p*-polarized beam (probe beam,

12.5mW/cm^2) counter-propagating to one of the writing beams was used to read the index grating formed in the material. The diffracted light intensity of the probe beam was detected by a photodiode and subsequently amplified with a lock-in amplifier. The diffraction efficiency η was calculated as the ratio of the intensities of the diffracted beam to the incident reading beam. Data were collected by a computer. The refractive indexes of the polymers were measured by using the Metricon Model 2010 Prism Coupler at 780nm.

Synthesis of M0. Thiophene (5.25g, 62.5mmol) was refluxed in 20ml hexane with TMEDA (21.77g, 187.4mmol), followed by dropwise adding *n*-butyl lithium (187.4mmol, 2.5M in hexane). The mixture was kept at reflux for 2.5h, then tributyltin chloride (49.2g, 151.2mmol) was dropwise added followed by another 0.5h of reflux. The mixture was then poured into water and the organic layer was separated and distilled under reduced pressure to yield monomer **M0** (22.84g, 55%). ^{1}H NMR (500MHz, $CDCl_3$, ppm): δ 0.89 (t, *J*=7.3Hz, 18H, CH_3), 1.10 (t, *J*=7.0Hz, 12H, CH_2), 1.33 (m, 12H, CH_2), 1.58 (m, 12H, CH_2), 7.35 (s, 2H).

M1. A mixture of compound **1** (1.00g, 0.938mmol)[10] and compound **2** (0.238g, 1.195mm0l) in 10ml ethanol was added a catalytic amount of NaOH (1.9mg, 0.047mmol, 15mg/ml aqueous solution). The mixture was allowed to reflux for 5 days. After the solvent removal, the residue was purified by flash chromatograph on silica gel (hexane:ethyl acetate = 6:1 v/v) to yield monomer **M1** as a dark blue/purple solid (1.031g, 88%). ^{1}H NMR (500MHz, $CDCl_3$, ppm): δ 0.88 (t, *J*=7.1Hz, 6H, CH_3), 1.25-1.34 (m, 72H, CH_2), 1.62 (m, 4H, CH_2), 1.74 (s, 6H, CH_3), 2.58 (t, *J*=8.1Hz, 4H, benzyl), 3.38 (t, *J*=7.9Hz, 4H, NCH_2), 6.62 (d, *J*=9.0Hz, 2H, aromatic protons), 6.71 (d, *J*=15.8Hz, 1H, trans double bond), 7.51 (d, *J*=9.0Hz, 2H, aromatic protons), 7.58 (d, *J*=15.8Hz, 1H, trans double bond), 7.58 (s, 1H, aromatic proton), 7.59(s, 1H, aromatic proton). ^{13}C NMR (125MHz, $CDCl_3$, ppm): 14.12, 22.68, 26.78, 27.00, 27.35, 29.29, 29.35, 29.38, 29.41, 29.49, 29.56, 29.65, 29.68, 30.18, 31.90, 39.81, 45.25, 51.32, 54.19, 93.52, 96.59, 100.33, 108.14, 111.62, 112.02, 112.82, 121.35, 132.58, 139.25, 144.73, 144.87, 148.26, 152.28, 174.06, 176.36. MS *m/z* calcd. from $C_{68}H_{104}N_4OI_2(M–H)^-$: 1246.40; Found: 1246.20.

M2. Prepared in a similar way as that of **M1**. Silica gel, hexane:ethyl acetate = 25:1 v/v. Yield: 65%. ^{1}H NMR (500MHz, $CDCl_3$, ppm): δ 0.83-0.88 (m, 12H, CH_3), 1.23-1.34 (m, 72H, CH_2), 1.62 (m, 4H, CH_2), 1.90 (m, 2H, CH_2), 2.08 (m, 2H, CH_2), 2.58 (t, *J*=8.0Hz, 4H, benzyl), 3.38 (t, *J*=7.8Hz, 4H, NCH_2), 6.65 (d, *J*=9.0Hz, 2H, aromatic protons), 6.73 (d, *J*=15.8Hz, 1H, trans double bond), 7.52 (d, *J*=9.0Hz, 2H, aromatic protons), 7.59 (d, *J*=15.8Hz, 1H, trans double bond), 7.58 (s, 1H, aromatic proton), 7.59(s, 1H, aromatic proton). ^{13}C NMR (125MHz, $CDCl_3$, ppm): 13.95, 22.46, 22.67, 27.00, 28.95, 29.27, 29.28, 29.34, 29.37, 29.41, 29.53, 29.56, 31.36, 31.90, 39.30, 39.80, 51.33, 53.48, 96.59, 100.32, 102.36, 108.56, 111.55, 112.07, 112.15, 112.81, 121.32, 132.54, 139.25, 144.72, 144.86, 147.34, 152.15, 172.38, 177.35. MS *m/z* calcd. from $C_{78}H_{124}N_4OI_2$ $(M–H)^-$: 1386.67; Found: 1386.40.

Polymerization. A typical polymerization procedure is listed below: A mixture of **M0** (0.316g, 0.477mmol) and **M1** (0.567g, 0.455mmol) in 5ml THF was added with $Pd(PPh_3)_2Cl_2$ (0.016g, 0.02mmol) as the catalyst. The mixture was kept at reflux with stirring for 2 days and then the catalyst was removed by filtration through Celite. The polymer was isolated through precipitation from methanol/hexane (2:1 v/v). Further purification was conducted by re-dissolving the polymer into chloroform, filtration and re-precipitation. The polymer was a dark blue viscous solid after being dried under vacuum at 40°C overnight. Yield: 0.464g (95%).

Reference:

18. Solymar, L.; Webb, D. J.; Grunnet-Jepsen, A. *The Physics and Applications of Photorefractive Materials* Clarendon Press, Oxford, 1996.
19. Moerner, W. E.; Silence, S. M. *Chem. Rev.* **1994**, *94*, 127.

20. Moerner, W. E.; Grunnet-Jepsen, A.; Thompson, C. L. *Annu. Rev. Mater. Sci.* **1997**, *27*, 585.
21. Yu, L.; Chan, W. K.; Peng, Z. H.; Gharavi, A. *Acc. Chem. Res.* **1996**, *29*, 13.
22. Wang, Q.; Wang, L.; Yu, L. *Macromol. Rapid Commun.* **2000**, *21*, 723.
23. Yu, L. *J. Polym. Sci. Part A: Polym. Chem.* **2001**, *39*, 2557.
24. Zhang, Y.; Burzynski, R.; Ghosal, S.; Casstevens, M. K. *Adv. Mater.* **1996**, *8*, 111.
25. Wang, Q.; Wang, L.; Yu, L. *J. Am. Chem. Soc.* **1998**, *120*, 12860.
26. Wang, Q.; Wang, L.; Yu, J.; Yu, L. *Adv. Mater.* **2000**, *12*, 974.
27. You, W.; Wang, Q.; Wang, L.; Yu, L. *Macromolecules* **2002**, *35*, 4636.
28. Wang, L.; Ng, M.-K.; Yu, L. *Appl. Phys. Lett.* **2001**, *87*, 700.
29. Hou, Z.;You, W.; Yu, L. *Appl. Phys. Lett.* (in press)
30. Ostroverkhova, O.; Wright, D.; Gubler, U.; Moerner, W. E.; He, M.; Sastre-Santos, A.; Twieg, R. T. *Adv. Funct. Mater.* **2002**, *12*, 621.
31. Bao, Z.; Chan, W. K.; Yu, L. *J. Am. Chem. Soc.* **1995**, *117*, 12426.
32. Moerner, W. E.; Silence, S. M.; Hache, F.; Bjorklund, G. C. *J. Opt. Soc. Am. B* **1994**, *11*, 320.
33. Wang, L.; Ng, M.-K.; Yu, L. *Phys. Rev. B.* **2000**, *62*, 4973.
34. Wortmann, R.; Poga, C.; Twieg, R. J.; Geletneky, C.; Moylan, C. R.; Lunquist, P. M.; DeVoe, R. G.; Cotts, P. M.; Horn, H.; Rice, J. E.; Burland, D. M. *J. Chem. Phys.* **1996**, *105*, 10637.
35. Bäuml, G.; Schloter, S.; Hofmann, U.; Haarer, D. *Opt. Comm.* **1998**, *154*, 75.

8. Molecular Diodes Based Upon Conjugated Diblock Co-oligomers

Our diblock copolymer projects has initially focused on demonstration of its rectification effect, which is an fundamental phenomenon that closely related to applications on molecular electronics and photovoltaic applications. We chose to synthesize molecules with one electron-rich and another electron deficient blocks. The designed molecule consists of an electron-rich bithiophene segment and an electron-poor bithiazole segment; they are efficient hole- and electron-transporting agents, respectively. Scheme 3 outlines the synthetic approach to the molecule. A thiol group was introduced to the thiophene end so that the diblock molecule can be assembled into monolayers on conductive gold surface for physical studies. The aromatic thiol is unstable and can easily be oxidized to disulphide. Fortunately, previous studies have established that disulphide compounds are equally effective in forming self-assembled monolayers (SAMs) directly on gold surfaces[28]. The chemical structure of diblock disulphide molecule **4** is shown in Scheme 3, along with that of a structurally similar reference compound **7** without the diblock structure. The latter compound was synthesized for a meaningful comparison of the electrical properties with that of the diblock oligomer **4**.

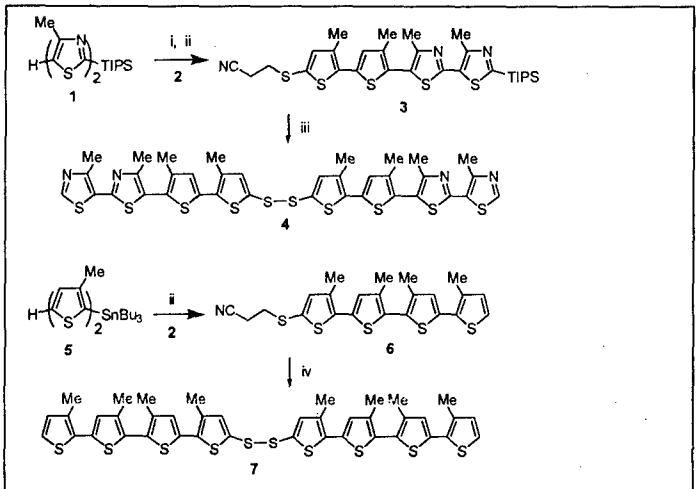

Reagents and conditions:
i. n-BuLi, THF, -78 0C, then Bu_3SnCl;
ii. Compound **2**, 2.5 mol% $Pd_2(dba)_3$, 20 mol% PPh_3, 50 mol% Cu_2O, DMF, 115 0C;
iii. TBAF (1.5 equiv), THF, rt.
iv. Compound **2**, 2.5 mol% $Pd_2(dba)_3$, 20 mol% PPh_3, DMF, 115 0C;

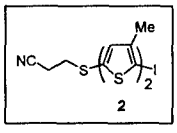

Scheme 3. Synthesis of molecular diodes for rectification effect.

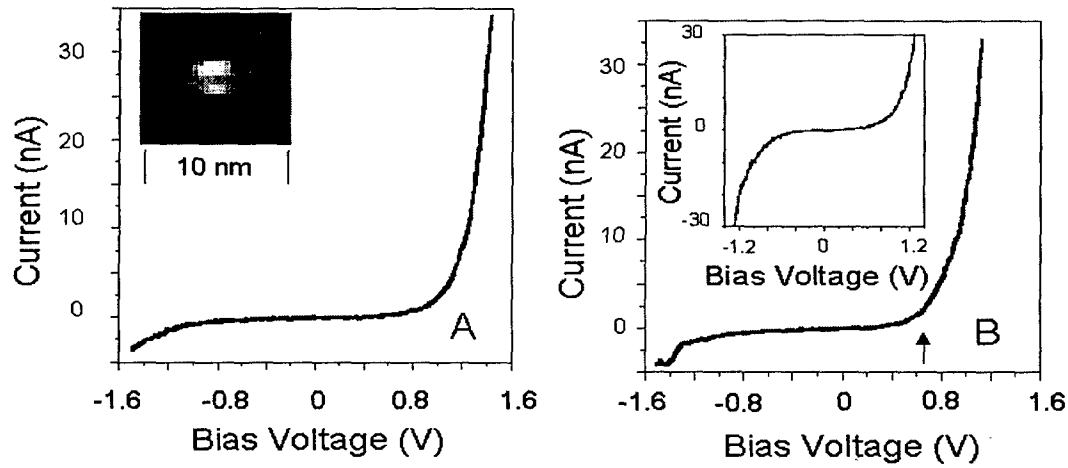

Figure 23: a. Current–voltage (*I–V*) characteristics of isolated molecules of diblock oligomer **4** inserted into preassembled monolayers of 1-decanethiol on Au/mica (the setpoint conditions +1000 mV and 2 pA). Inset: constant-current STM image of the mixed monolayers on Au/mica. Same tunneling conditions were used to acquire the image. The bright spots (~5 Å higher than background) correspond to molecules derived from **4**.

b. *I–V* characteristics of pure monolayers of diblock oligomer **4** on Au surface (the setpoint conditions +600 mV and 2 pA). Inset: *I–V* characteristics of pure monolayers of reference oligomer **7** with bipolar turn-on voltage ~±0.8 V (the setpoint were +600 mV and 2 pA).

The current-voltage (*I-V*) characteristics of the monolayers of the diblock molecule were investigated by scanning tunneling spectroscopy (Nanoscope III, Digital Instruments). After a stable STM scan was obtained, the feedback loop for the STM control was briefly interrupted. The Pt/Ir STM tip (grounded to zero potential) was then held at a constant position above the film, the tip-sample separation being determined by the impedance used, which typically ranged from 60 to 300 GΩ in these experiments. High impedance was used throughout the STM experiment to avoid large fluctuations in tip movement and prevent mechanical damage to the sample surface. The voltage was then ramped from positive to negative bias while the current tunneling through both the air gap and the molecule was recorded.

First, to probe the rectifying effect due to single molecules, molecules **4** were inserted into SAM of alkanethiol host.[5,27] The bright spots in the inset to Fig. 23a is the constant-current STM image of the molecule 4 inserted into preassembled monolayers of decanethiol. The bright spots all over the monolayers of decanethiol are very uniform in size (~2 nm diameter) and constant-current height (~5–6 Å from background). STS studies were performed on top of both the bright spots and the surrounding decanethiol molecules. The *I–V* characteristics determined for single molecules of **4** is depicted in Fig. 23a. Pronounced *I–V* asymmetry is observed for these single molecules, with turn-on voltage at around +1.0 V, whereas the corresponding tunnel current at –1.0 V remains at a low value. In contrast, the decanethiol background showed a near-perfect symmetric *I–V* curve, the current is more than an order of magnitude smaller than that of diblock molecule **4**. The differential conductance curve (obtained from data in Fig. 23a) is shown in Figure 3. A turn-on voltage of ~1.0 V on the positive side can also be deduced.

The monolayers assembled from pure disulphide **4** were investigated with optical ellipsometry and scanning tunnelling microscopy (STM). Ellipsometry provides a macroscopic

film thickness of 16.0 ± 0.5 Å, compared to a theoretical end-to-end distance of 18.6 Å based on fully optimized geometry of conjugated thiol derived from **4** using quantum chemical method. This result indicates that the molecules adopt an average tilt angle of ~30° from the surface normal, as schematically shown in Fig. 1. A large current-voltage (*I-V*) asymmetry was also consistently observed in the SAM of pure compound **4** (Fig 23b). The threshold voltage for significant current increase on the positive sample bias was about +0.75 V, a measure of tunneling barrier for electron injection from STM tip to LUMO of the molecule. The difference in turn-on voltage observed here (+0.75 V) and that found for mixed monolayers of **4** (+1.0 V) is due to difference in tunneling resistance (bias of 600 mV for data shown in Fig. 2b and +1000 mV for Fig. 23a). To illustrate the asymmetry in conductivity on both positive and negative biases, the differential conductance (d*I*/d*V*) versus voltage relationship was considered and is shown in Fig. 24 (inset). The large asymmetry in conductance is evident with threshold turn-on voltage of ~+0.8 V.

In order to confirm that the *I–V* asymmetry was not due to work function difference between gold substrate and Pt/Ir tip or to artifacts caused by poorly controlled tip-sample interaction, monolayers of a reference oligomer **7** were prepared and studied accordingly by STS under the same conditions as for compound **4**. The *I–V* curves obtained for monolayers of **7** exhibited nearly perfect symmetric behavior over a fairly large bias range (inset in Fig. 23b). This is clear evidence that the rectifying effect observed in monolayers of disulphide **4** is due to the intrinsic diblock nature of the molecule.

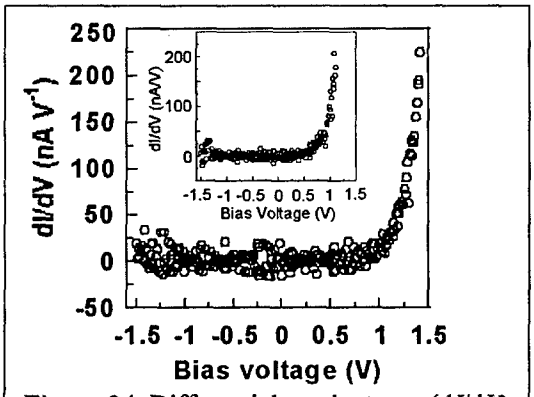

Figure 24: Differential conductance (d*I*/d*V*) versus voltage relationship for the *I–V* data shown in Fig. 23a (isolated molecule **4**). Inset: d*I*/d*V* versus voltage plot of the *I–V* data shown in Fig. 23b.

Methods

Monolayer formation. To prepare monolayers for STM or ellipsometry studies, gold substrates (~1000 Å) thermally evaporated on mica or silicon wafer supports were immersed in chloroform solutions of disulphide 1 or 2 ($\sim 0.8 \times 10^{-3}$ mol l^{-1}) at room temperature for 24 h. The samples were rinsed with hexanes, ethanol and chloroform, blown dried with argon, and stored under N_2. To insert disulphide 1 into insulating preassembled pure monolayers of decanethiol, Au substrates on mica were immersed in ethanolic solutions of decanethiol (2×10^{-3} mol l^{-1}) at room temperature for 18 h, rinsed with ethanol and placed in a chloroform solution of 1 ($\sim 0.33 \times 10^{-3}$ mol l^{-1}) at room temperature for 8 h.

Monolayer characterization. STM images were recorded with a Nanoscope III (Digital Instruments, Santa Barbara, CA, USA) in the constant-current mode, operated under ambient conditions, and STS was performed using the program routines. Electrochemically etched Pt/Ir tip (Molecular Imaging, Phoenix, AZ, USA) were used for both STM and STS studies. The I-V curves are the average value of measurements in the same spot. Ellipsometry measurements were performed with a Gaertner L116C single-wavelength optical ellipsometer equipped with a He-Ne laser operating at the wavelength of 632.8 nm with incidence angle of 70°. An index of refraction of 1.55 was assumed for the film thickness calculations.

1. Riordan, M. & Hoddeson, L. *Crystal Fire: The Birth of the Computer Age* (W. W. Norton & Company, New York, 1997).
2. Aviram, A. & Ratner, M. Molecular rectifiers. *Chem. Phys. Lett.* 29, 277–283 (1974).
3. Jortner, J. & Ratner, M. (eds) *Molecular Electronics* (Blackwell Science, Oxford, 1997).

4. Joachim, C., Gimzewski, J. K. & Aviram, A. *Nature* 408, 541–548 (2000).
5. Bumm, L. A. *et al. Science* 271, 1705–1707 (1996).
6. Reed, M. A., Zhou, C., Muller, C. J., Burgin, T. P. & Tour, J. M. *Science* 278, 252–254 (1997).
7. Schön, J. H., Meng, H. & Bao, Z., *Nature* 413, 713–716 (2001).
8. Schön, J. H., Meng, H. & Bao, Z. *Science* 294, 2138–2140 (2001).
9. Gudiksen, M. S., Lauhon, L. J., Wang, J., Smith, D. C. & Lieber, C. M. *Nature* 415, 617–620 (2002).
10. Huang, Y. *et al. Science* 294, 1313–1317 (2001).
11. Bachtold, A., Hadley, P., Nakanishi, T. & Dekker, C. *Science* 294, 1317–1320 (2001).
12. Tans, S. J., Verschueren, A. R. M. & Dekker, C. *Nature* 393, 49–52 (1998).
13. Martel, R., Schmidt, T., Shea, H. R., Hertel, T. & Avouris, P. *Appl. Phys. Lett.* 73, 2447–2449 (1998).
14. Derycke, V., Martel, R., Appenzeller, J. & Avouris, P. *Nano Lett.* 1, 453–456 (2001).
15. Geddes, N. J., Sambles, J. R., Davis, D. J., Parker, W. G. & Sandman, D. J. *Appl. Phys. Lett.* 56, 1916–1918 (1990).
16. Pomerantz, M., Aviram, A., McCorkle, R. A., Li, L. & Schrott, A. G. *Science* 255, 1115–1118 (1992).
17. Martin, A. S., Sambles, J. R. & Ashwell, G. J. *Phys. Rev. Lett.* 70, 218–221 (1993).
18. Fischer, C. M., Burghard, M., Roth, S. & Klitzing, K. V. *Europhys. Lett.* 28, 129–134 (1994).
19. Lee, I., Lee, J. W. & Greenbaum, E. *Phys. Rev. Lett.* 79, 3294–3297 (1997).
20. Stabel, A., Herwig, P., Müllen, K. & Rabe, J. P. *Angew. Chem. Int. Ed. Engl.* 34, 1609–1611 (1995).
21. Dhirani, A., Lin, P.-H., Guyot-Sionnest, P., Zehner, R. W. & Sita, L. R. *J. Chem. Phys.* 106, 5249–5253 (1997).
22. Metzger, R. M. *et al.. J. Am. Chem. Soc.* 119, 10455–10466 (1997).
23. Collier, C. P. *et al. Science* 285, 391–394 (1999).
24. Wong, E. W. *et al. J. Am. Chem. Soc.* 122, 5831–5840 (2000).
25. Chen, J., Reed, M. A., Rawlett, A. M. & Tour, J. M. *Science* 286, 1550–1552 (1999).
26. Chen, J. *et al. Appl. Phys. Lett.* 77, 1224–1226 (2000).
27. Donhauser, Z. J. *et al. Science* 292, 2303–2307 (2001).
28. Nuzzo, R. G., Fusco, F. A. & Allara, D. L. *J. Am. Chem. Soc.* 109, 2358–2368 (1987).
29. Seminario, J., Zacarias, A. G. & Tour, J. M. *J. Am. Chem. Soc.* 122, 3015–3020 (2000).
30. Sellers, H., Ulman, A., Shnidman, Y. & Eilers, J. E. *J. Am. Chem. Soc.* 115, 9389–9401 (1993).

9. Synthesis of New Diode Molecules and Their Sequential Assembling to Control Electron Transport

The above diode molecules opened a new direction for our diblock copolymer subproject. It shows the potential for making impact on molecular electronics. However, the molecule described above has only one terminal sulfur atoms for connection with gold surfaces. To explore the use of such diode molecules in potential electronic devices, it is necessary to equip this thiophene –thiazole diblock oligomer with two different terminal thiol groups that can be sequentially connected to gold electrodes; thereby the rectifying direction can be predetermined with the known molecular orientation between the two electrodes. Further research is aimed at synthesis of diode molecules with asymmetrically protected thiols groups so that the rectifying direction of diode molecules can be controlled in a two-terminal circuit configuration through sequential assembling process. To the best of our knowledge, this is the first example of showing control of the electron transport by controlling the orientation of diode molecules between two electrodes.

We synthesized two thiophene –thiazole diblock oligomers with two different thiol-protected end groups. The orientation of the diblock structure between gold electrodes was controlled through a sequential deprotection and immobilization procedure (deprotection a / self assembly / deprotection b / Au nanoparticles). It was found from electron transport studies that the rectifying effect of the resulting assembly was indeed controlled by the orientation of the molecules.

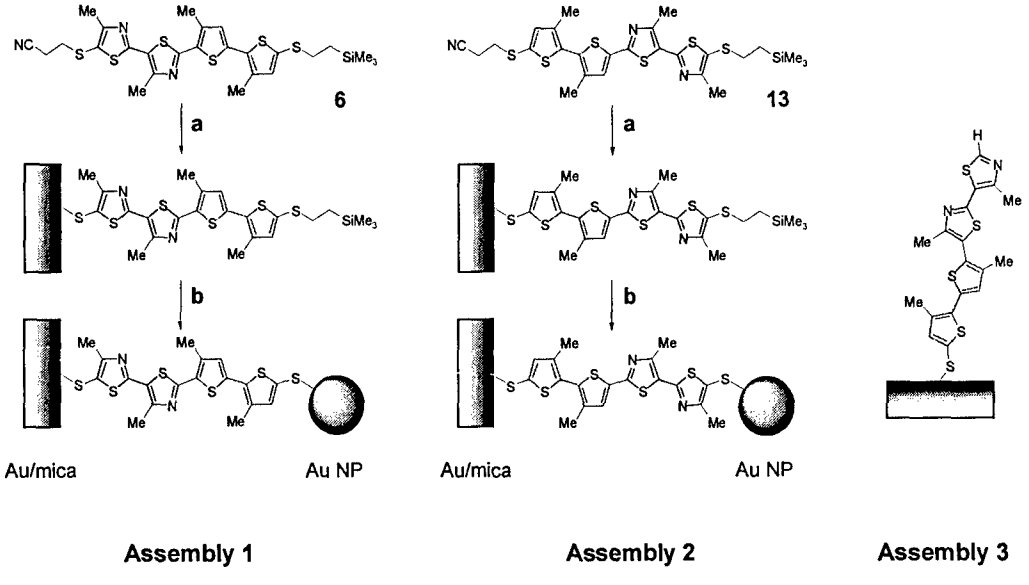

Scheme 4: Preparation of assemblies 1 and 2. a. NaOEt, THF, gold substrate; b.TBAF, THF, Au nanoparticles. Assembly 3 (ref 5b).

The synthetic procedure for the molecule in assembly **A3** was reported previously.[5] Introducing another thiol group to the compound in **A3** proved to be infeasible due to the tautomerism between thiol and thione. However, we found that thiolation at 5-position in the

thiazole molecule can be achieved. Thus, compounds **6** and **13** were designed and their syntheses are outlined in Scheme 5. The two thiol-protection groups used are cyanoethylene $-S-CH_2CH_2CN$ (CNE) and trimethylsilylethylene $-S-CH_2CH_2SiMe_3$ (TMSE). The former can be readily deprotected to free thiol under basic condition while the latter is stable even under very basic conditions such as butyllithium but labile to fluoride-mediated cleavage.[6] Our synthetic strategy was to build TMSE-thio protecting group at the beginning, taking advantage of its inertness to basic conditions, and then put the CNE-thio protection group later in the synthesis. The TMSE-thio group was first attached to the dithiophene unit through the dithiophene iodide **1** based on a general method for aryl-sulfur bond formation using copper (I) as catalyst.[7] After Stille coupling with the dithiazole block **4**, the diblock molecule with TMSE-thio protecting group **5** was prepared. The last step was to introduce the CNE-thio group at the other end to form **6** based on a previously used procedure.[5b]

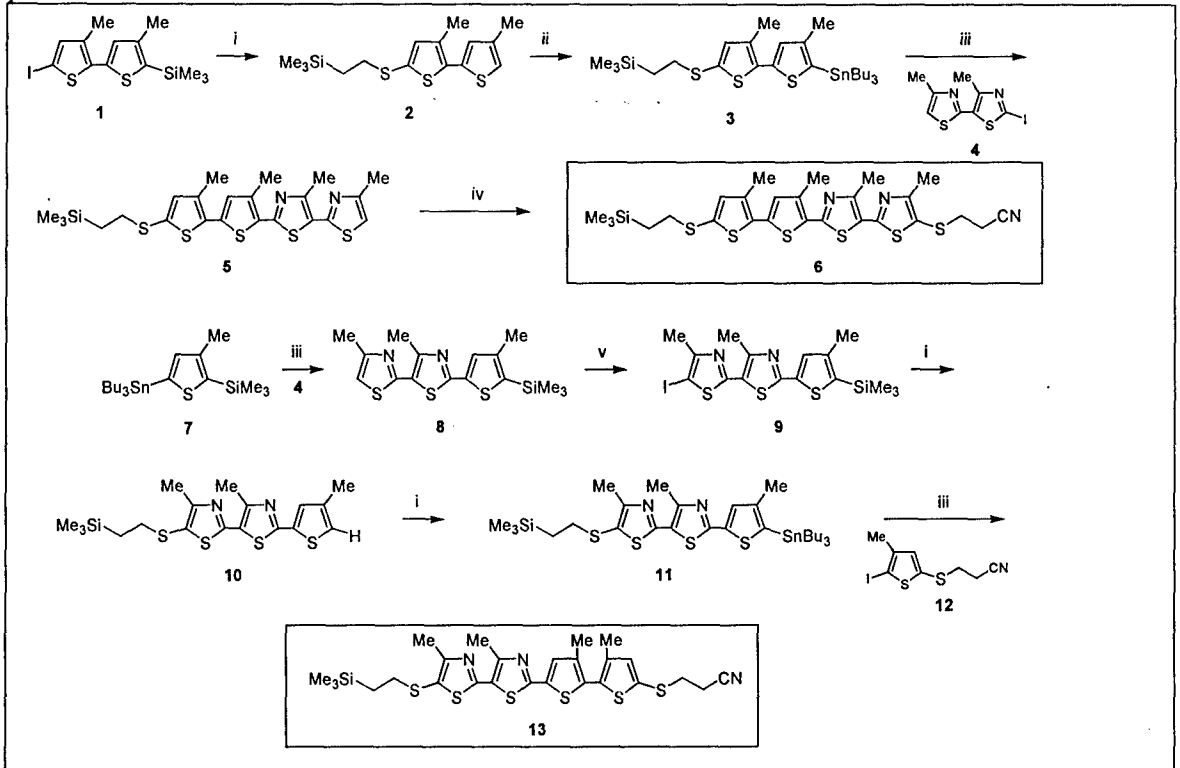

Scheme 5: Syntheses of compound **6** and **13**. i). a. $Me_3SiCH_2CH_2SH$, CuI, NaOtBu, neocuproine, toluene, 110°C; b. TFA. ii) a. BuLi, -78 °C; b. Bu_3SnCl. iii). $Pd_2(dba)_3$, PPh_3, Cu_2O, DMF, 130-135°C. iv). a. BuLi, -78°C; b. S_8; c. $BrCH_2CH_2CN$. v). a. BuLi, THF, -78°C. (b). I_2.

Originally, we planned to deprotect TMSE-thio and CNE-thio groups on compound **6** in two different sequences so that the diode molecule could be immobilized to electrodes with different orientations. Experiments showed that first deprotection of TMSE group would also simultaneously eliminate the CNE group. However, deprotection of CNE-thio group first worked well with TMSE-thio group intact. Thus, the sequential deprotection procedure- deprotection of CNE-thio group first and then TMSE-thio group-was applied. In order to reverse the molecular orientation between

electrodes, compound **13** was then synthesized. Compound **13** has the similar diblock structure as compound **6,** but with the two different thio-protection groups switched in positions (Scheme 5). Since it is difficult to functionalize the 2-position of dithiazole unit after TMSE-thio protection group was added on the 5'-position, we chose first to couple dithiazole **4** with one thiophene unit with its 2-position protected to form compound **8**, then attached the TMSE-thio protection group using the same coupling reaction described above. Finally another thiophene unit with a built-in CNE-thio protection group was connected through Stille coupling reaction to make compound **13**. ^{1}H and ^{13}C spectra are consistent with the expected structures. Mass spectra show mass of M^{+} about 604.9 for both compounds **6** and **13**.

The orientation of the diblock structure between gold electrodes was controlled through a sequential deprotection and immobilization procedure (deprotection a / self assembly / deprotection b / Au nanoparticles) as described in Scheme 4. First, the CNE-thio group was deprotected in situ to free thiol by sodium ethoxide /ethanol and the target molecules were self-assembled onto the gold substrate. Then the TMSE-thio group was deprotected with TBAF solution in THF and treated with freshly made gold nanoparticles (NP). Thus the diode molecules were connected with both ends to gold electrodes and ready for electron transport study. The assemblies **A1** and **A2**, prepared from molecule **6** and **13**, respectively, were shown in Scheme 4.

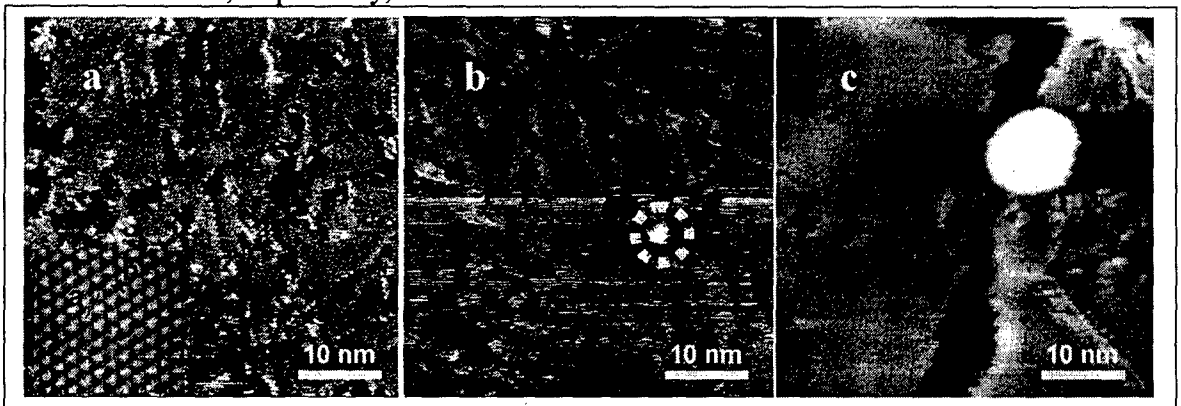

Figure 26: Constant current STM topography of a dodecanethiolate SAM on Au (111)/mica, before (a) and after (b) the insertion of 6; the molecule is shown as bright spot and indicated by a circle. c. The image of the surface after attachment of Au nanoparticle to the top termini of **6**. The area showed is 50 × 50 nm^2, STM imaging conditions: V_{bias} = +1.0 V, I_t = 1 pA).

To investigate the charge transport on the single molecules, monolayers with isolated diode molecules are needed. We utilized Au(111) dodecanthiolated self-assembly monolayer (DDT SAM) as the substrate, into which the molecules **6** and **13** were inserted. Figure 26a shows the STM image of DDT SAM on Au(111) surface as a highly ordered structure. High resolution images (inset in Figure 1a) reveal a hexagonal packing with a averaged distance between the nearest and next-nearest neighbor spacing (represented by *a* and *b* respectively) of ~ 0.5 nm and ~ 0.9 nm, which correspond to the characteristic $(\sqrt{3} \times \sqrt{3})$ R30° absorbate overlayer on Au(111).[8] Figure 26b shows a STM image taken on the DDT SAM after insertion of molecules **6**. The bright spot (indicated by a circle) in Figure 26b is the constant-current STM image of the molecule **6** with the TMSE-thio protecting group on the top. The images are reproducible through different scans. The intensity of the bright spots change sporadically in agreement with the stochastic behavior reported for single molecules inserted in alkanethiolate SAM.[9] The shape and size of the spots are constant and the size is averaged about 1.8 nm, which is similar to other single molecules inserted in

alkylthiol matrix.[10] Under the insertion conditions used in this work, the bright spots are probably single molecules; however, we cannot rule out the possibility of formation of aggregates. According to the data available in the literature, the orientation of DDT is defined by a tilt angle of 30°.[8] Since molecules of assemblies **A1** and **A2** are located in the defects of the DDT SAM, we assume both assemblies have the same orientation as DDT SAM on the gold surface. After the TMSE-thio protecting groups were removed, Au NPs were attached to the exposed terminal thiol groups. Figure 1c shows the STM image of this Au-**S-6-S**-Au assembly **A1**. The apparent diameter of the Au NP is in the range between 9-11 nm. A separate TEM micrograph of NP showed an average diameter of 8 nm.[11] The enlargement in the size of single molecules and NP can be attributed to the combination of electronics factors and tip convolution effects.

Electron transports for the assemblies **A1** and **A2** prepared in scheme 4 were investigated by scanning tunneling spectroscopy (STS). It has been demonstrated that gold NP can be immobilized to the surface thiol groups in symmetrical alkyldithiol monolayers assembled on Au substrate and I-V behaviors of the assembly can be readily measured by Scanning Probe Microscopy.[12] Figures 2 summarized the averaged I(V) data for assembly **A1** (Figure 27a) and **A2** (Figure 27b). The gap conditions used to define the tip-sample separation are -0.5 nA and -0.1 nA at -1.5 V, respectively. The STS spectra for **A1** clearly showed asymmetric I-V behavior with higher current at negative bias potential than at positive one. The average rectification ratio (RR) is 0.19 (for easy comparison, 1/RR is was used in Figure 27a), where RR is defined by RR = I(+1.5V)/I(-1.5V).[13] Opposite rectifying behaviors were found for assembly **A2** with an average RR of 4.8. To demonstrate the reproducibility of the I(V) curves for different NP on the SAM monolayer, the inset histograms showed the statistical distribution of 1/RR for **A1** and RR for **A2** for the different NP measured. The RR range is 2-7 for A1 while the 1/RR range for **A2** is 3-7. The ranges in both cases can be attributed to different conformations of the molecules into the SAM defects. The statistical histogram analyses were based on measurements taken on ~50 different immobilized single Au NP for each assembly. The I(V) data for each NP is the average of ~100 individual I(V) curves, each of which composes of 256 points, while each point has been averaged 3-5 times by the software.

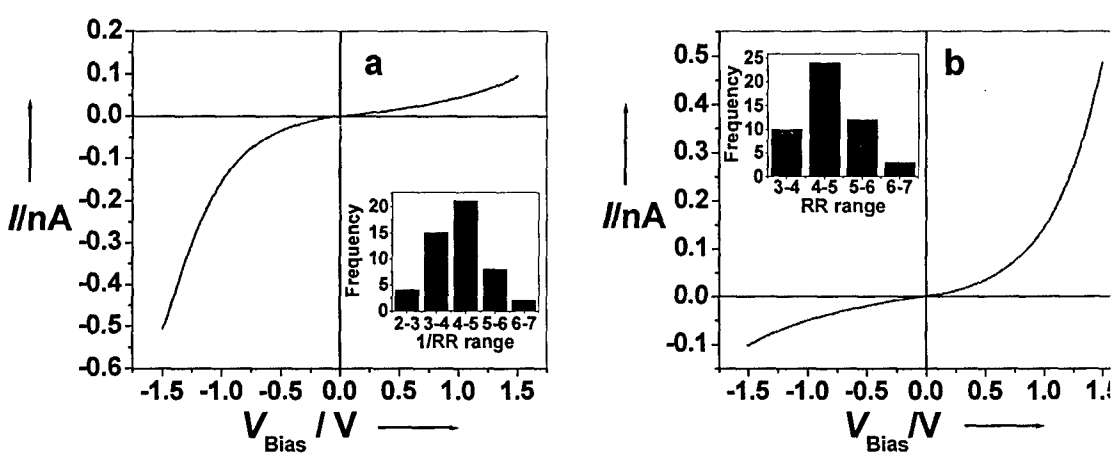

Figure 27: Averaged I(V) curves measured over ~50 different gold nanoparticles at V_{bias} = -1.5 V for a) assembly **A1** (I_t = -0.5 nA,) and b) assembly **A2** (I_t = -0.1 nA).

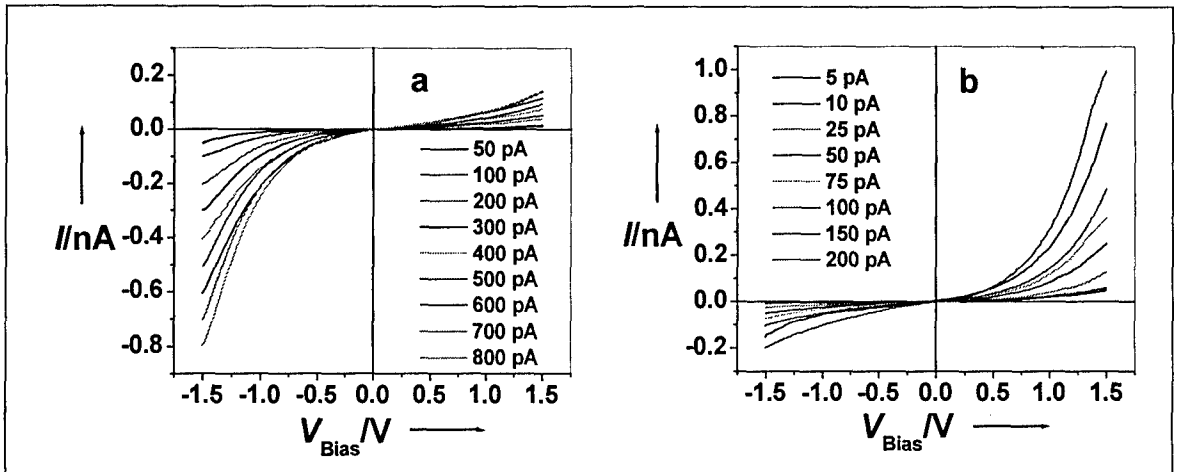

Figure 3: I(V,z) data taken at different current set points for a V_{bias} of -1.5 V for: a) assembly **A1** and b) assembly **A2**.

We also changed the current set points (distance between the STM tip and the Au NP), to see the behavior of the junction under different gap conditions. Figure 28 shows the I(V) curves obtained at different current set points for assembly **A1** and **A2**. The opposite asymmetric I(V) behaviors for **A1** and **A2** were observed consistently with various current set points. Though the interplay of two junctions together with the charging of the NP can change the symmetry of the I(V) curve,[14] the contribution should be always in the same direction. In our case the opposite asymmetry between **A1** and **A2** ruled out any significant contribution from such effect.

Since the opposite rectifying behavior for **A1** and **A2** also rules out any contribution in the asymmetry originated from the measurement setup, the rectifying effect observed should be an intrinsic property of the molecules. Though the position of one side methyl group on one thiophene unit was different in compounds **6** and **13**, which may affect the twist angle of the conjugation and thus electron delocalization, we believe that the determining factor is the dipole orientation of the thiophene-thiazole diblock rather than the slight difference in the side methyl group. The results are consistent with our previous results from the assembly **A3** in Scheme 1. Assembly **A3** has the same dipole orientation as assembly **A2**. Preliminary calculations at the HF/G-31G level showed that the component along the molecule axis is 1.68 and 1.54 Debye for molecules **6** and **13**, respectively.

[1] A. Aviram, M. Ratner, *Chem. Phys. Lett.* **1974**, *29*, 277-283.

[2] J.-P. Launay, *Chem. Soc. Rev.* **2001**, *30*, 386-397.

[3] R. M. Metzger, *Chem. Rev.* **2003**, *103* (9), 3803-3834.

[4] C. Joachim, J. K. Gimzewski, A. Aviram, *Nature* **2000**, *408*, 541-548.

[5] a) M.-K. Ng, L. Yu, *Angew. Chem. Int. Ed.* **2002**, *41*, 3598-3601. b) M.-K. Ng, D.-C. Lee, L. Yu, *J. Am. Chem. Soc.* **2002**, 124, 11862-11863.

[6] M. B. Anderson, M. G. Ranasinghe, J. T. Palmer, P. L. Fuchs, *J. Org. Chem.* **1988**. *53*, 3127-3129.

[7] C. G. Bates, R. K. Gujadhur, D. Venkataraman, *Org. Lett.* **2002**, *4*, 2803-2806.

[8] a) C. A. Widring, C. A. Alves, M. D. Porter, *J. Am. Chem. Soc.* **1991**, *113*, 2805-2810. b) C. A. Alves, E. L. Smith, M. D. Porter, *J. Am. Chem. Soc.* **1992**, *114*, 1222-1227.

[9] a) Z. J. Donhauser, B. A. Mantooth, K. F. Kelly, L. A. Bumm, J. D. Monnell, J. J. Stapleton, D. W. Price Jr, A. M. Rawlett, D. L Allara, J. M. Tour, P. S. Weiss, *Science* **2001**, *292*, 2303-

2307. b) G. K. Ramachandran, T. J. Hopson, A. M. Rawlett, L. A. Nagahara, A. Primak, S. M. Lindsay, *Science* **2003,** *300*, 1413-1416. c) R. A. Wassel, R. R. Fuierer, N. Kim, C. B. Gorman, *Nano Lett.* **2003**, *3*(11), 1617-1620.

[10] P. S. Weiss, L. A. Bumm, T. D. Dunbar, T. P. Burgin, J. M. Tour, D. L. Allara, *Ann. NY Acad. Sci.* **1998**, *852,* 145-168.

[11] D. I. Gittins, F. Caruso, *Angew. Chem. Int. Ed.* **2001**, *40*, 3001-3004.

[12] a) M. Dorogi, J. Gomez, R. Osifchin, R. P. Andres, R. Reifenberger, *Phys. Rev. B* **1995**, *52*(12), 9071-9077. b) D. I. Gittins, D. Bethell, D. J. Schiffrin, R. J. Nichols, *Nature* **2000**, *408*, 67-69. c) X. D. Cui, A. Primax, X. Zarate, J. Tomfohr, O. F. Sankey, A. L. Moore, T. A. Moore, D. Gust, G. Harris, S. M. Lindsay, *Science* **2001**, *294*, 571-574.

[13] R. M. Metzger, T. Xu, I. R. Peterson, *J. Phys. Chem. B* **2001**, *105*(30), 7280-7290.

[14] A. E. Hanna, M. Tinkhan, *Phys. Rev. B* **1991**, *44*, 5919-5922.

10. Concluding Remarks:

Our research in this grant period is characterized productivity and new discoveries. Our photorefractive materials project identified new form of photorefractive materials, namely monolithic materials. Detailed structure/property studies revealed new features and point to the approaches to the improvement of PR performances. We discovered the dramatic effect of trapping molecule on PR properties, which can be significant for future optimization of PR materials. We must also point out that the key issue in organic PR materials is the slow response time. It seems to be an intrinsic problem because organic materials usually have a rather low charge carriers' mobility. The response time, of course, is a function of applied field. High field will lead to fast response time. The dilemma is the high field also can lead to dielectric breakdown of the materials and bring heavy cost to power supply system. A better system that has a combined properties is the one developed in our lab, which contains oligothiophene and an NLO chromophores.

Our diblock copolymer project demonstrated pronounced rectification effect in an asymmetric diblock co-oligomers, the fundamental feasibility of diblock copolymers as the PV materials. Photocell is a diode that is driven by photo energy. It laid foundation for future development of these materials for solar cell application. We have succeeded in synthesizing a new version of diblock copolymers that exhibit fast charge separation rate and slow charge recombination process. Detailed studies on solar cell is in progress.

In the past grant period, we are also successful in educating new generation of scientist related to DOD's mission. Four graduate students partially supported by this grant received their Ph.D degrees and two postdoctoral associates worked on this project. Two of them went to academic institution as assistant professors and others found positions in industrial labs.

We thank AFOSR for kind support of our research.

---

[i] See supporting information for plots of cross-section showing the apparent size of the Au-**S-6-S**-TMSE and Au-**S-6-S**-Auarrays displayed in Figure 2b.

AFRL-SR-AR-TR-05-

REPORT DOCUMENTATION PAGE

0310

1. REPORT DATE *(DD-MM-YYYY)*	2. REPORT TYPE	3. DATES COVERED *(From - To)*
07/13/2005	Final Technical Report	05/01/2002-04/30/2005

4. TITLE AND SUBTITLE
Searching for Better Photorefractive and Photovoltaic Materials

5a. CONTRACT NUMBER

5b. GRANT NUMBER
F49620-02-1-0218

5c. PROGRAM ELEMENT NUMBER

6. AUTHOR(S)
Luping Yu

5d. PROJECT NUMBER

5e. TASK NUMBER

5f. WORK UNIT NUMBER

7. PERFORMING ORGANIZATION NAME(S) AND ADDRESS(ES)

Department of Chemistry
The University of Chicago
5735 South Ellis Av.
Chicago, IL 60637

8. PERFORMING ORGANIZATION REPORT NUMBER

9. SPONSORING / MONITORING AGENCY NAME(S) AND ADDRESS(ES)
AFOSR/PKC
875 Randolph Street
Arlington, VA 22203-1954

NL

10. SPONSOR/MONITOR'S ACRONYM(S)

11. SPONSOR/MONITOR'S REPORT NUMBER(S)

12. DISTRIBUTION / AVAILABILITY STATEMENT
This document has been approved for public release and sale, its distribution is unlimited.

13. SUPPLEMENTARY NOTES

14. ABSTRACT
This report summarizes the research effort for the grant period as indicated above on search for better photorefractive materials. New synthetic approaches and new materials with much improved photorefractive properties have been developed. Detailed discussion and description are described in this report. It was also reported the development of conjugated diblock co-oligomers for rectifying effect, which is the fundamental requirement for photovoltaic applications.

15. SUBJECT TERMS

16. SECURITY CLASSIFICATION OF:			17. LIMITATION OF ABSTRACT	18. NUMBER OF PAGES	19a. NAME OF RESPONSIBLE PERSON
a. REPORT	b. ABSTRACT	c. THIS PAGE			Luping Yu
					19b. TELEPHONE NUMBER *(include area code)* 773-702-8698

7-26-05